UNIVERSITY of
BRADFORD

Library

The University of Bradford Institutional Repository

http://bradscholars.brad.ac.uk

Link to publisher's version: *http://dx.doi.org/10.1016/j.desal.2017.01.020*

Citation: Alsadaie SM and Mujtaba IM (2017) Dynamic modelling of Heat Exchanger fouling in multistage flash (MSF) desalination. Desalination. 409: 47-65.

Dynamic Modelling of Fouling in Multistage Flash (MSF) Desalination

Salih M. Alsadaie and Iqbal M. Mujtaba*

*Chemical Engineering Division, School of Engineering, University of Bradford, Bradford BD7 1DP, UK

E-mail: I.M.Mujtaba@bradford.ac.uk

ABSTRACT

Fouling on heat transfer surfaces due to scale formation is the most concerned item in thermal desalination industry. Here, a dynamic fouling model is developed and incorporated into the MSF dynamic process model to predict fouling at high temperature and high velocity. The proposed dynamic model considers the attachment and removal mechanisms in the fouling phenomena with more relaxation of the assumptions such as the density of the fouling layer and salinity of the recycle brine. While calcium sulphate might precipitate at very high temperature, only the crystallization of calcium carbonate and magnesium hydroxide are considered in this work. Though the model is applied in a 24 stages brine recycle MSF plant, only the heat recovery section (21 stages) is considered under this study. The effect of flow velocity and surface temperature are investigated. By including both diffusion and reaction mechanism in the fouling model, the results of the fouling prediction model are in good agreement with most recent studies in the literature. The deposition of magnesium hydroxide increases with the increase in surface temperature and flow velocity while calcium carbonate deposition increases with the increase in the surface temperature and decreases with the increase in the flow velocity.

Kay words: MSF; scale formation; dynamic fouling model; calcium carbonate; magnesium hydroxide.

1. Introduction

Fouling, due to scale formation, is the accumulation of undesirable layer of solid materials at the heat transfer surface. With time, these materials continuously build up fouling film causing an increase in the thermal resistance and reduce the performance of process equipment [1]. The performance of multistage flash (MSF) desalination plants is mainly affected by the condition of heat transfer surfaces, therefore, scales on these surfaces by seawater containing salts can impede the rate of heat transfer and reduce the efficiency of the heat transfer process resulting in poor performance of the plant. Moreover, increasing the layer thickness of the scales results in narrowing the tubes pass and consequently increase the energy consumption (of pumps) to maintain a constant flow rate. Seawater always has the tendency for scale formation and fouling problems due to dissolved salts and finely suspended solids. As highlighted in Mujtaba [2, 3], at high temperature, water with soluble

salts allows deposits to form scale which can reduce the heat transfer rate and can increase specific energy consumption and operating costs. This can cause frequent shutdowns of the plant for cleaning. Due to the fouling tendency, the heat transfer equipment are overdesigned with allowable 20 to 25% excess in heat transfer surface area thus increased capital cost. This results in an increase of about 30% of the total cost [4].In thermal desalination process such as MSF, the scale formation is mainly caused by precipitation of calcium carbonate ($CaCO_3$), and at higher temperature, magnesium hydroxide $Mg(OH)_2$. Both of them are commonly referred to as alkaline scales. Non-alkaline scale such as calcium sulphate ($CaSO_4$), on the other hand, is also considered to be the most common scales found in MSF process [5]. Nevertheless, Anhydrite sulphate scale ($CaSO_4$) would be expected to form at temperature above 40 ^{o}C due to its low solubility (Figure 1) [6], most of the calcium sulphate scale in thermal units is hemihydrate [7, 8]. However, there is large agreement among the MSF fouling researchers that $CaSO_4$, in any forms, precipitates in MSF plants at temperature above 120 ^{o}C [5]. Since, in this work, the highest temperature in the condensing tubes is considered to be less than 112 ^{o}C, the precipitation of $CaSO_4$ is neglected in this work and only the precipitation of $CaCO_3$ and $Mg(OH)_2$ are considered.
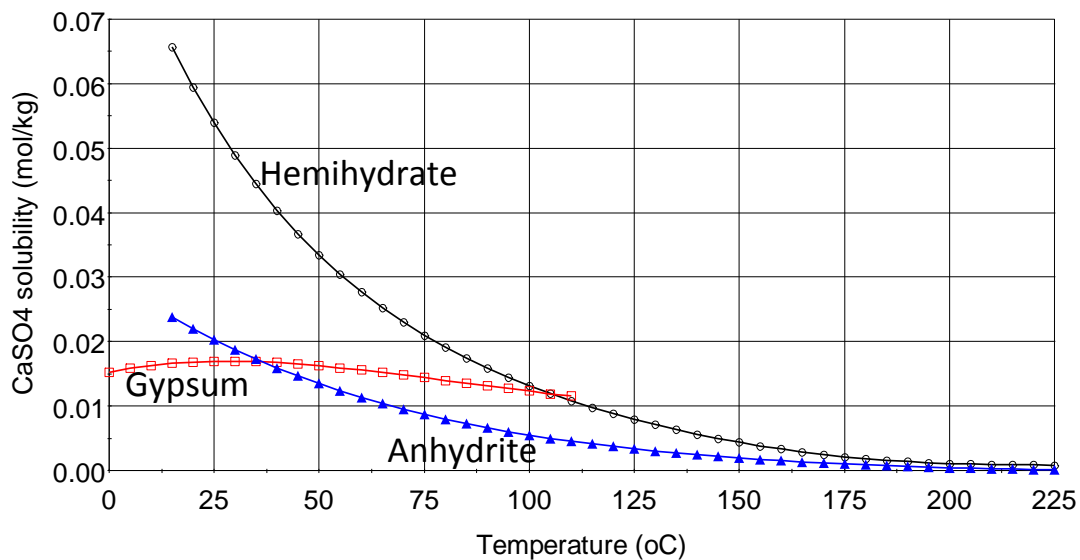

Figure 1: The solubility of $CaSO_4$ in its three different forms [9]

The fouling phenomena on hot surfaces is affected strongly by number of factors such as time, surface temperature, velocity of the bulk, diffusion rate of the ions, bulk composition, solubility of the scale species and the pH of the seawater. For carbonate systems, the amount of carbonate species is related to the pH as shown in Figure 2 [10]. The increase in the seawater pH causes the condition of calcium carbonate to be super-saturation which in turn results in scale deposit. Therefore, controlling pH value is required to prevent excessive carbonate scale formation. Calcium sulphate, however, is pH independent and tends to deposit in different forms once its solubility limitation exceeds [11]. Hofling et al. [12] reported that the saturation index for $CaSO_4$ is almost constant between pH 4 and pH 10.
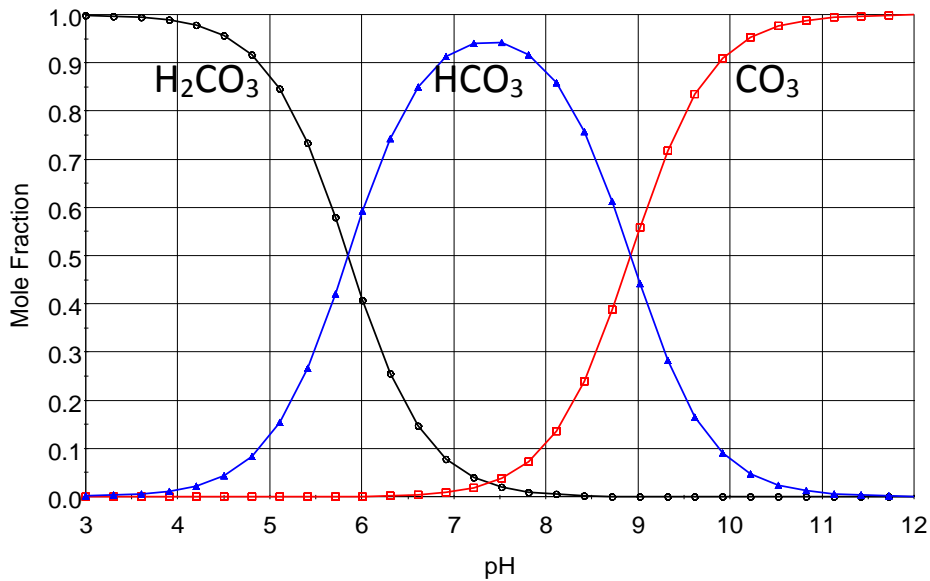
Figure 2: Mole fraction of CO_2, HCO_3 and CO_3 as a function of pH in carbonate system at (T = 25 ^{o}C and salinity = 35 g/l) [10].

Although a good amount of studies were carried out on the experimental study of scaling, corrosion, scale formation at heat transfer surface is still very complex problem to understand and it is the weakest point in the design of heat transfer equipment. One of the early attempts to model fouling behaviour was conducted by Kern and Seaton [13]. They confirmed that the fluid velocity plays an important role in limiting the increase of the fouling thickness by considering a constant deposit rate and increasing removal rate, so that the process of fouling reaches steady state when the removal rate becomes equal to the deposition rate [14]. Although it is a simple model and ignored several parameters that may be responsible for the scale formation, it is considered to be the basic model on which further models have been developed. Hasson et al. [15] developed a diffusion model to control only $CaCO_3$ scale deposition in heat transfer surface. Experimental data from double pipe heat exchanger was used to validate their model and found out that the scale growth of $CaCO_3$ varies with Reynold's number and is only slightly dependent on surface temperature. Later, Gazit and Hasson [16] developed a kinetic model to study the parameters that affect the $CaCO_3$ scale formation in film flow desalination process. Using a heated aluminium tube, the main parameter to be examined was the effect of evaporation temperature on the kinetic of scale formation.

Taborek et al. [17] developed fouling model to study the $CaCO_3$ scaling on cooling tower water. It was assumed that the deposit rate depends on the flow velocity. However, the model was criticised on having many unknown variables and no experimental data were presented to estimate these variables. Hasson et al. [18] developed an ionic diffusion model to predict the fouling rates of $CaCO_3$. Later, in 1981, Hasson modified his model to predict the crystallisation rate of $CaSO_4$ [19]. Müller-Steinhagen and Branch [20] modified Hasson's ionic diffusion model to calculate the scaling rate of $CaCO_3$ in double pipe heat exchanger. However, the drawback of these models is that they did not account for removal rate since

they relied on the Hasson's assumption that the equation is valid for flow velocity less than 0.8 m/s.

Mubarak [21] developed a kinetic model for scale formation based on experimental data to study the reaction mechanism leading to $CaCO_3$ and calculate the deposition rate with and without the presence of antiscalant at fixed TBT (90 ^{o}C). Brahim et al. [22] developed a model to calculate the $CaSO_4$ scale formation using computational fluid dynamics (CFD) code FLUENT. The results showed a good agreement with experimental data. Bohnet [23], describes a fouling model which involves deposit rate correlation of second order reaction of $CaSO_4$ and combines diffusion rate and reaction rate to eliminate the unknown concentration of the calcium and carbonates ions at the solid-liquid surface. The model describes the transport, deposition and removal of the scale. Mwaba et al. [24] developed a semi-empirical correlation to predict the nucleation phase of the fouling scale in heat exchanger by introducing roughness enhancement factor. It was assumed that for the case of $CaSO_4$, the deposit rate was controlled by the surface reaction and the diffusion rate was neglected assuming that the concentrations of the ions in the bulk and at the solid-liquid surface are the same. The model was validated via experiment showing good agreement between the model prediction and the experimental data.

Al-Rawajfeh [25] developed a model combining mass transfer and chemical reaction to calculate the release of CO_2 and its relation to the deposition of $CaCO_3$ in once through MSF process. Segev et al. [26] developed a kinetic diffusion model that allows the study of multicomponent transport of all ionic species involved in carbonic fouling system. The effect of pH level on the deposition rate was studied using simplified and rigorous models. Based on Brahim's work [22], Zhang et al. [27] developed a generic CFD model to predict the fouling behaviour of $CaSO_4$. The model avoided the simplification step adopted by Brahim et al. [22] by coupling solution domain with fouling layer domain through bi-directional transfer.

Despite the large aforementioned publications on the fouling process, most of these models have been developed and studied on their own but have not been a part of the MSF process models. Moreover, most of the works were conducted on heat exchanger, which can be found in many industries as stand-alone unit. However, in MSF plants, the flashing stages can be considered as a series of connected heat exchangers where the fouling behaviour becomes more complex and hard to predict due to the continuous change of the temperature and salinity

While the majority of the developers of the MSF models use a constant fouling factor in their studies, which may lead to excessive or unnecessary overdesign, only a handful of studies focused on the modelling (or attempts to modelling) of scale formation in MSF process. Moreover, most of the experiments used a velocity less than 1 m/s where in the MSF process however, the velocity is between 1.5 m/s and 2.3 m/s [28].

During their comprehensive study to compare different types of antiscalant at fixed TBT and concentration factor, Hamed and Al-Otaibi [29] estimated the fouling factor as the difference

between the overall heat transfer coefficient at scaled condition and at clean condition. A regression analyses was used to obtain a linear correlation that describe the fouling factor. Hawaidi and Mujtaba [30] developed a linear dynamic model for brine heater fouling to study the impact of fouling with seasonal variation of seawater temperatures. Said et al. [31] extended Hawaidi and Mujtaba's study to include the effect of fouling in the stages using a steady state MSF model. These regression models do not consider a number of variables that may have critical effects on the fouling behaviour and consequently inaccurate results would be expected [32]. Al-Rawajfeh et al. [8] extended the Al-Rawajfeh's work [25] to develop a fouling model for MSF process. The model was implemented on brine recirculation and once through MSF process with and without antiscalant. The results were compared to experimental and simulation results from literature. However, the model only accounted for the deposit rate and neglected the removal rate.

Though the above few publications are well established and seem to be very promising, all of them neglected the dynamic variation of seawater salinity and temperature. In brine recirculation MSF process in particular, the temperature and salinity of the recycled brine change with the change in fouling rate. Therefore, in this work, a dynamic fouling model will be developed to investigate the behaviour of fouling in the MSF condensing tubes with increasing of cooling water temperatures from stage to another. The model will be based on previous models but it will be coupled with MSF model to predict the fouling behaviour in the stages condensing tubes.

2. Process Description

A conventional brine recirculation MSF-BR process is shown in Figure 3. The process consists of a brine heater and a large number of flashing stages divided in heat recovery section (HRS) and heat rejection section (HRJ). The seawater (W_s) enters the condenser tubes of the HRJ at temperature (T_{cw}) and leaves at a temperature (T_1). The outlet stream of the HRJ is split into two parts; one part is rejected to the sea (C_W) and the other part is fed to the last stage as make-up (F). The recycle brine (Rec) is drawn from the last stage of the HRJ at (T_5) and it is fed to the last stage of the HRS where it is gradual heated as it passes through the tubes from one stage to another by exchanging the thermal energy from the flashing vapour in each stage to a temperature of (T_2). In the brine heater, the preheated seawater temperature is further raised to the maximum allowable temperature (T_3) called the TBT. The heat energy required to increase the brine temperature to the TBT is normally supplied by steam coming from an electrical power plant. At this point, the flashing brine from the brine heater enters the first stage of the HRS flash chamber through an orifice or weir. Here the ambient pressure is reduced in such a way that the water will become superheated and flashed off to give pure vapour which is condensed on the condenser tubes and is collected in the distillate tray across the stages. As the flashing brine would be still hot enough to boil again at slightly lower pressure, the flashing brine flows into the next stage and the flashing process is then repeated all the way down the plant. The brine then leaves the recovery section at temperature (T_4) and rejection section at (T_5) where part of the brine goes to blow down (B_D) and the other part (Rec) is withdrawn from the last stage and then recycled to the HRS [33].

The seawater (W_s) and the recycle brine water (Rec) flow through bundles of large number of pipes, which are connected by water boxes, in counter current direction of the brine flow leaving the brine heater (Figure 4). The temperature of the seawater and recycle brine water increases gradually from T_{cw} to T_1 and from T_5 to T_2 respectively due to the condensation process inside the flashing chambers.
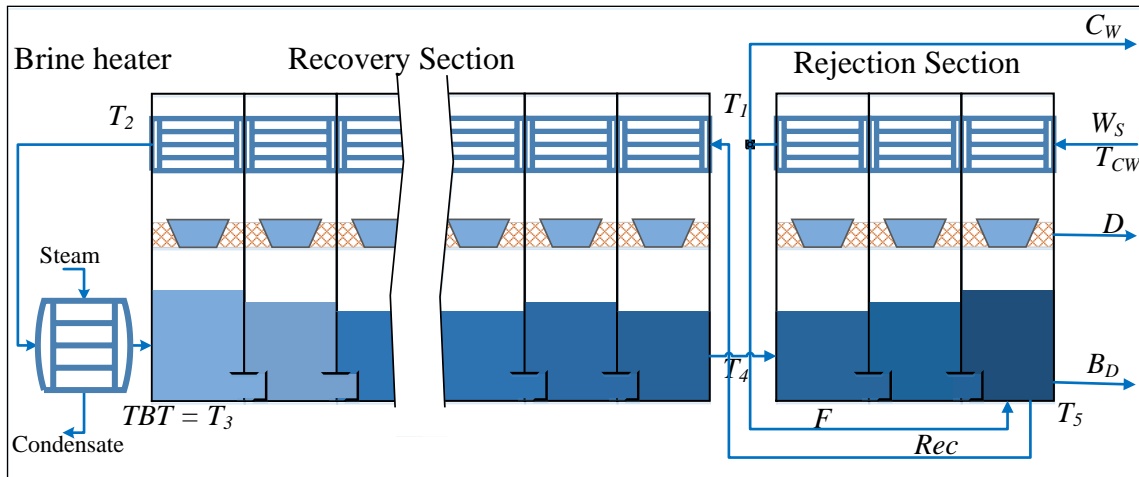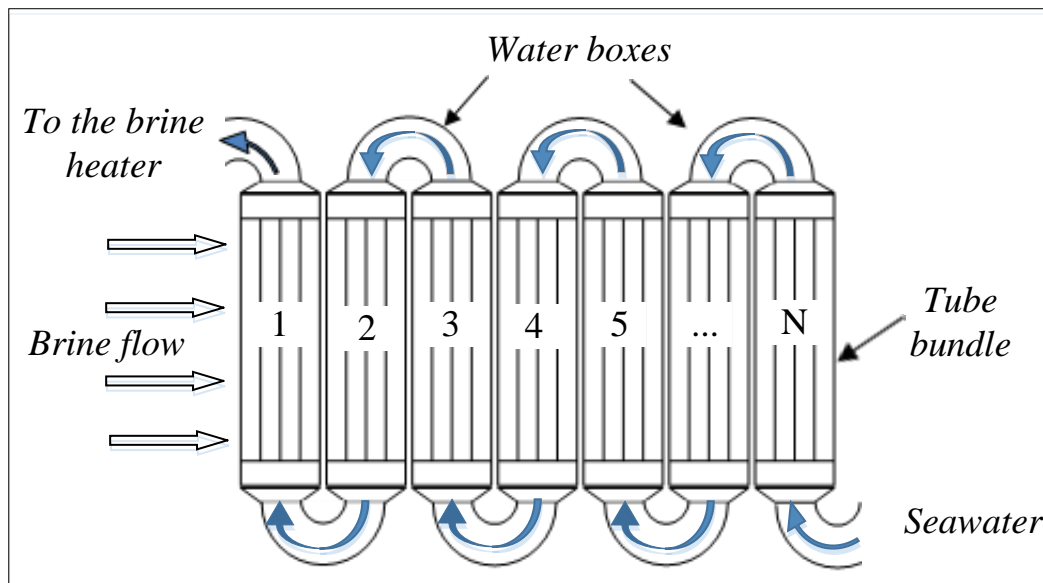

Figure 3: Schematic of MSF-BR process

Figure 4: Schematic of tubes bundles and water boxes of MSF process

The deposited scale, mainly $CaCO_3$ and $Mg(OH)_2$, starts to accumulate in different amount according to their concentration and temperature of the inner side of the tube surface. Stage number 1, for example, is expected to have the highest amount of scale due the high temperature and low solubility concentration. Although, the fresh seawater intake has higher Ca^+_2 concentration, no high deposit is likely expected to form in the rejection section stages due to low temperature. In summer period, the fresh intake water enters the last stage (stage 24) at $T_s = 32\ ^oC$ and leaves the rejection section from stage 22 at $T_1 = 40\ ^oC$.

However, in a continuous precipitation of fouling, the situation becomes more complex as there is a continuous change in heat flux, temperature and salinity. The continuous deposition of the fouling on the inner surface of the tubes reduces the heat flux to the brine inside the tubes and thus results in temperature drop. Moreover, this reduction in heat flux leads to less vapour to be condensate around the tubes and consequently increase the vapour volume and the pressure inside the chamber. Since the main concept of MSF process is the evaporation of water under vacuum, this increase in the pressure inside the chamber may lead to less vapour to flash and as result, the temperature of the brine and the vapour increase. Since the brine inside the tubes is recirculated from the last stage, its temperature increases with time causing an increase in the temperature inside the tubes. To make the situation more complex, the reduction of the amount of evaporation from the brine leads to decrease in the brine salinity, which in turn affect the solubility of the calcium carbonate in seawater.

3. Fouling Model

During the fouling model building process, the following important assumptions are considered in this work:

- Lumped distribution of fouling deposit along the tubes is considered.

- Pressure drop between inlet and outlet of the tubes is neglected.

- Volumetric flow through the tubes as assumed constant and therefore, the velocity change due to change in cross sectional area is considered.

- The salinity variation due to the change in the amount of condensate is considered.

Depending on the process variables and fouling mechanism, four observed fouling behaviour can be developed to describe the rate of fouling as shown in Figure 5 [17].

- Linear rate: a straight line indicates a constant growth rate of deposit with time and with negligible removal rate;
- Falling rate: a curved line indicates increase in the growth rate of deposit with increase in the removal rate after some time;
- Asymptotic rate: a curved line indicates increase in the growth rate of deposit as well as gradual removal to reach a steady state with time when both rates equal each other; and,
- Saw-tooth shape rate: deposition rate exhibits a general increase trend punctuated with periodic decrease due to the shedding of fouling deposits. The deposit then builds up and detached continuously.
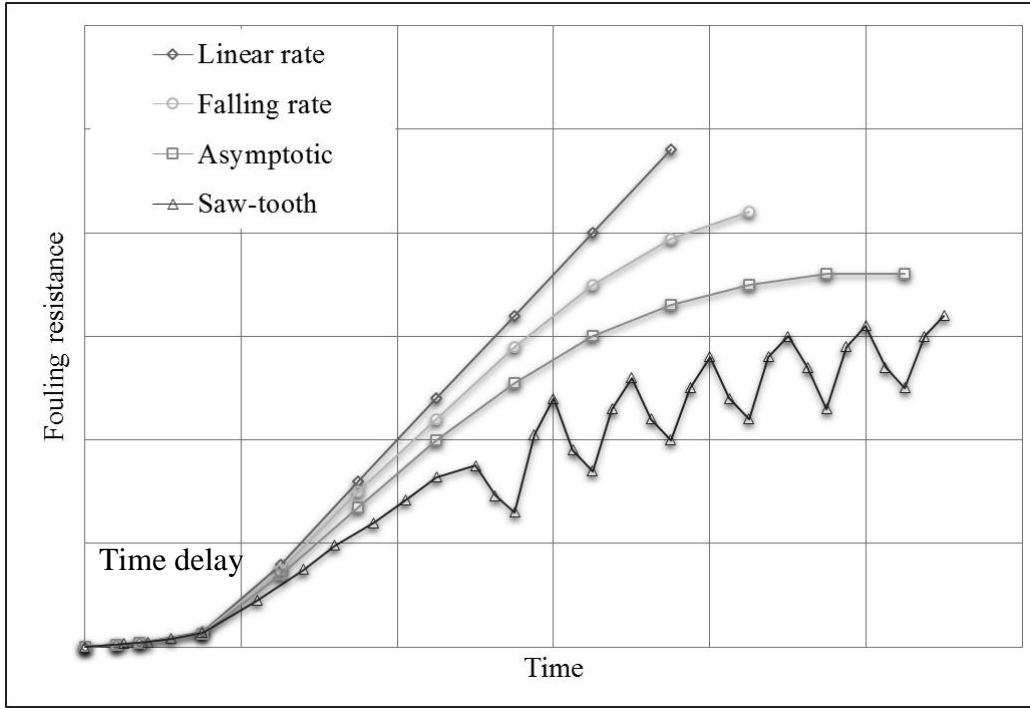
Figure 5: Possible fouling resistance versus time curves [6].

3.1 Deposit rate

Based on the above descriptions of fouling behaviour rate, a good model that can be close to real behaviour is the model that consider the growth and removal rate of the scale. The net deposit rate can be calculated as the difference between the total deposition rate and the removal rate.

$$\frac{dm_f}{dt} = m_d - m_r \tag{1}$$

Where m_f , m_d and m_r are the net deposit mass rate, the total deposit mass rate and the removal mass rate per unit area respectively. The total mass deposit rate can be described using ions diffusion transport rate and/or surface reaction rate as shown in Figure 6.

The first step of scale formation is the transportation of species toward the heated surface as a result of concentration difference between the bulk phase (C_b) and the solid-liquid surface (C_i). The ions diffusion transport rate can be written as follows:

$$\frac{dm_d}{dt} = k_D(C_b - C_i) \tag{2}$$

Where k_D is the mass transfer coefficient, C_b is the concentration of the ions in the fluid (bulk phase) and C_i is the concentration of the ions at the solid-liquid surface.
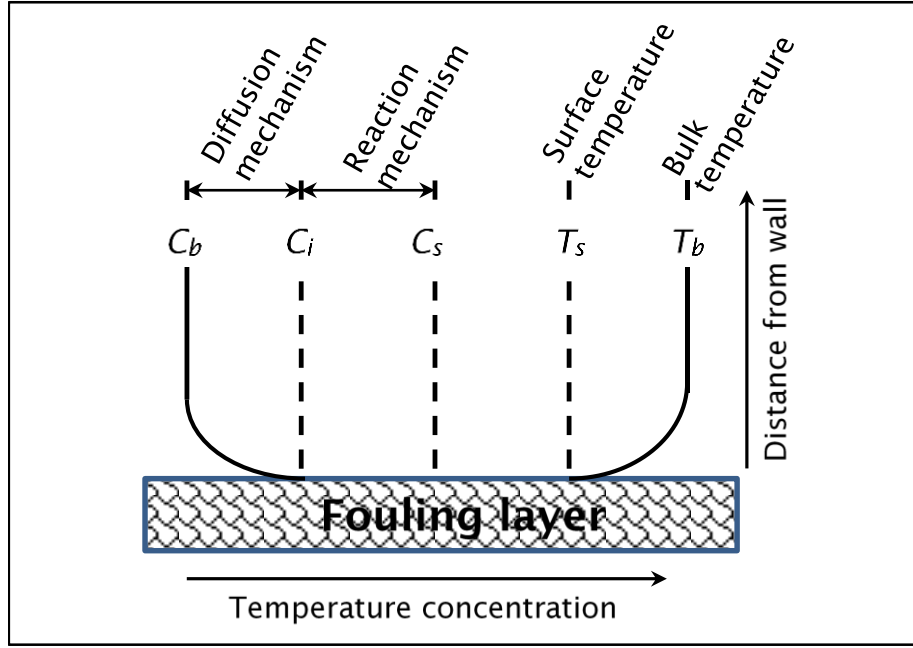
Figure 6: Concentration and temperature profiles at the heat transfer surface [15]

The second step is the accumulation of these transported species on the crystal layer at the heated surface as a result of concentration difference between the solid-liquid surface (C_i) and the saturation concentration (C_s).. The deposit rate from the reaction process can be calculated as follows:

$$\frac{dm_d}{dt} = k_r(C_i - C_s)^n \qquad (3)$$

Where k_r is the reaction rate constant, C_s is the saturation concentration and n is reaction order. For the deposition of $CaCO_3$, the reaction order is assumed to be of second order reaction as it correspond to the number of ions (Ca^{2+} and CO_3^{2-}) [22]. Due to the difficulty of estimating the concentration of the ions at the solid-liquid surface (C_i), most of the work in the literature assumed that all the species are transported to the surface and thus the surface reaction mechanism is considered to be the main controller of the deposit rate. Helalizadeh et al. [11] and Fahiminia et al. [34] reported that at low velocity, the fouling is controlled by diffusion rate while at high velocity, the controller mechanism changes to be reaction rate. Moreover, Najibi et al. [7]assumed that the fouling process is controlled by diffusion mechanism when the velocity bellow 0.9 m/s. Also, Andritsos et al. [35] reported large indication of diffusion controlled process when they tested two velocities below 0.9 m/s on the activation energy. Augustin and Bohnet [36] and Paakkonen et al. [37] reported that the crystallization of $CaCO_3$ is reaction controlled. If the reaction mechanism is assumed to be the controlled mechanism, then equation (3) can be used to describe the deposit rate in heated surface areas at appropriate surface temperature and species concentration. The concentration driving force in equation (3) has been described by Hasson et al. [18] based on the concentrations and the solubility product K_{sp} of calcium carbonate and the reaction order of the formation of calcium carbonate was assumed as first order reaction ($n = 1$) as reported by Hasson et al. [15].

9

$$\frac{dm_d}{dt} = k_r([Ca].[CO_3] - K_{sp}) \tag{4}$$

Where the solubility product of calcium carbonate can be defined as

$$K_{sp} = [Ca^{2+}].[CO_3^{2-}]$$

Similar form of the concentration driving force in Equation (3) can be found in the literature to describe the crystallization rate of calcium carbonate or concentration reduction of calcium ions. Smith and Sweett [38] presented six forms to describe the concentration driving force gradient term (C_b-C_s) with reaction order ranges from 1.8 to 2.14 between 30 $^{\circ}$C and 90 $^{\circ}$C.

In order to include the diffusion rate, Bohnet [39] combined equations (2 and 3) by reformulation and summation to eliminate the unknown interfacial concentration C_i to develop an equation (Equation 5) for precipitation of calcium sulphate where the deposition rate depends on both diffusion and reaction rates. Helalizadeh et al. [40] and Paakkonen et al. [41] used Bohnet's equation to calculate the crystallization fouling of calcium carbonate on heat exchange surface. Thus, in this work, the deposition of calcium carbonate will be assumed to depend on both diffusion and reaction mechanism according to the following equation:

$$\frac{dm_d}{dt} = \beta \left[\frac{1}{2}\left(\frac{\beta}{k_r}\right) + (C_b - C_s) - \sqrt{\frac{1}{4}\left(\frac{\beta}{k_r}\right)^2 + \left(\frac{\beta}{k_r}\right)(C_b - C_s)} \right] \tag{5}$$

The mass transfer coefficient β can be calculated as a function of the Sherwood number (Sh) and the diffusion coefficient (D).

$$\beta = \frac{Sh \times D}{D_h} \tag{6}$$

Sherwood number can be calculated as following.

$$Sh = 0.034 \times Re^{0.875} \times Sc^{1/3} \tag{7}$$

Where Re is the Reynolds number, Sc is the Schmidt number, D_h is the hydraulic diameter. The diffusion coefficients for calcium and carbonate system species can be found in Segev et al.[26].

Reynolds number and Schmidt number can be calculated from the following equations.

$$Re = \frac{\rho_w \times v \times D_h}{\mu_w} \tag{8}$$

$$Sc = \frac{\mu_w}{\rho_w \times D} \tag{9}$$

Pääkkönen et al [41] suggested to include the effect of flow velocity by introducing time scaling factor to equation (3) to become:

$$\frac{dm_d}{dt} = k_r(C_i - C_s)^n \times \frac{\mu_w}{\rho_w V^2} \tag{10}$$

Where V is the friction velocity and it can be calculated as following:

$$V = \sqrt{\frac{\tau_f}{\rho_w}} \tag{11}$$

The τ_f is the surface shear stress of the bulk flow and ρ_w is the density of the fluid. The surface shear stress can be calculated using friction factor according to the follow equation:

$$\tau_f = f \rho_w \frac{v^2}{2} \tag{12}$$

Thus, the combination of diffusion and reaction mechanism model (equation 5) becomes:

$$\frac{dm_d}{dt} = \beta \left[\frac{1}{2} \left(\frac{\beta \rho_w V^2}{k_r \mu_w} \right) + (C_b - C_s) - \sqrt{\frac{1}{4} \left(\frac{\beta \rho_w V^2}{k_r \mu_w} \right)^2 + \left(\frac{\beta \rho_w V^2}{k_r \mu_w} \right) (C_b - C_s)} \right] \tag{13}$$

The reaction rate constant (k_r) depends on the surface temperature (T_s) according to the Arrhenius equation.

$$k_r = k_{r0} \times e^{(-Ea/RT_s)} \tag{14}$$

Where k_{r0}, Ea, and R stand for pre-exponential constant, reaction activation energy, gas constant and the fouling surface temperature respectively. It is to be noted here that prior to the fouling, the T_s is equal to the temperature of the tubes wall. However, as the thickness of the fouling layer increases, the temperature of the wall, the temperature of the fouling surface and the salinity of the recycle brine are due to a change as described in section 2.

Although calcite has slightly lower saturation concentration, the aragonite is more favourable to deposit. X-ray analysis of Helalizadeh et al. [11] study revealed that 99% of the calcium carbonate scale was aragonite. Thus, it is assumed that the calcium carbonate scale in MSF tubes is aragonite. To calculate the solubility product of aragonite, Plummer and Busenberg [42] developed an equation to calculate the solubility product as a function of the temperature. However, in MSF process, the salinity of the brine water changes continuously due to the variation of the temperature and heat flux through the walls of the tubes. The solubility product, K_{sp} increases with pressure and salinity and decreases with temperature [1].Thus, it is important to consider the effect of activity coefficient of the seawater species. The solubility product of calcium carbonate is given by

$$K_{sp} = K_{sp}^0 / (\gamma_{Ca} \cdot \gamma_{CO3}) \tag{15}$$

Where $K^o{}_{sp}$ of aragonite can be calculated using Plummer and Busenberg's equation:

$$Log(K_{sp}^0) = \left[-171.9773 - 0.077993 \times T_s + \frac{2903.293}{T_s} + 71.595 \times Log(T_s) \right] \tag{16}$$

Where γ is the activity coefficient of a component, k_{sp} is in molar units and T_s is in Kelvin.

The activity coefficient can be calculated using extended WATEQ-Debye-Huckel's equation as citied by Al-Anezi and Hilal [1].

$$Log(\gamma_i) = -Az_i^2 \frac{\sqrt{I}}{1+Ba_i\sqrt{I}} + b_iI \tag{17}$$

Where A is the Debye-Huckel parameter, z is the charge of the ion, B is temperature dependent parameter, a_i and b_i are ion specific parameters of component i and I is ionic strength which is defined by:

$$I = \frac{1}{2}\sum z_i^2 m_i \tag{18}$$

The crystal growth of magnesium hydroxide is associated with the consumption of magnesium ions and thus it can be calculated by estimating the decrease in the magnesium concentration from the following equation [43].

$$-\frac{dMg^{2+}}{dt} = k_r\{([Mg^{2+}].[OH^-]^2)^{\frac{1}{3}} - [K_{sp}]^{1/3}\} \tag{19}$$

Thus,

$$\frac{dm_{Mg(OH)2}}{dt} = -\frac{dMg^{2+}}{dt} \tag{20}$$

Unlike calcium carbonate, the deposit rate of magnesium hydroxide is assumed to be first order reaction. The calculation of the solubility product K_{sp} for magnesium hydroxide is similar to that one for calcium carbonate. (The reader should be aware of the mass and molar units when applying equations 19 and 20).

For Mg(OH)$_2$, the solubility product can be calculated from the following correlation [44]:

$$Log(K_{sp}^0) = 14.723 - \frac{3472.3}{T_s} - 0.04642 \times T_s \tag{21}$$

Since this model is applied in MSF plant that contains several stages working as heat exchangers, the bulk concentration, C_b, is decreased throughout the stages due to the precipitation process and thus the calcium ions of the following stages are calculated based on the following equations:

$$Ca_{(j+1)} = Ca_{(j)} - CaCO_{3(j)} \tag{22a}$$

$$Mg_{(j+1)} = Mg_{(j)} - Mg(OH)_{2(j)} \tag{22b}$$

Where j presents the number of stages and the ions are in mole units.

The total deposit rate of CaCO$_3$ and Mg(OH)$_2$ can be evaluated as the sum of both substances.

$$\frac{dm}{dt} = \frac{dm_{CaCO3}}{dt} + \frac{dm_{Mg(OH)2}}{dt} \qquad (23)$$

To calculate the other seawater species such as (HCO_3, CO_3, CO_2, OH, H) at different temperatures and salinities, a carbonate system equations which has been described in [8] can be used. For given initial total alkalinity (TA) and initial total carbon dioxide (TC), the value of seawater pH can be obtained by iteration the following equation

$$[H^+]^3 + (TA + K_1)[H^+]^2 + (TA.K_1 + K_1.K_2 + K_w - TC.K_1)[H^+]$$

$$-K_1.K_2.\frac{K_w}{[H^+]} + (TA.K_1.K_2 - K_1.K_w - 2.TC.K_1.K_2) = 0 \qquad (24)$$

The pH is the negative logarithm of H$^+$. K_1, K_2 are the first and the second dissociation constants for carbonic acid respectively. K_w is the dissociation constant for water at a specific ions strength and temperature. These constants can be calculated based on the following equations [45]:

$$Log(K_1) = 2.18867 - 2275.035/T_s - 1.468591 \times Ln(T_s) + (-0.138681 -$$
$$9.33291/T_s) \times S^{0.5} + 0.072648 \times S - 0.00574938 \times S^{1.5}$$
(25)

$$Log(K_2) = -0.84226 - 3741.1288/T_s - 1.437139 \times Ln(T_s) + (-0.128417 -$$
$$24.41239/T_s) \times S^{0.5} + 0.1195308 \times S - 0.0091284 \times S^{1.5}$$
(26)

$$Log(K_w) = 148.9802 - 13847.26/T_s - 23.6521 \times Ln(T_s) + (-5.977 - 118.67/T_s +$$
$$1.0495 \times Ln(T_S)) \times S^{0.5} - 0.01615 \times S$$
(27)

Where S is a salt concentration in g/l. After knowing the hydrogen ion concentration (H$^+$) from equation (24), the unknown concentrations of the carbonic system species (OH$^-$, HCO$_3^-$, CO$_3^-$ and CO$_2$) can be calculated according to the following equations [18, 20]:

$$[OH^-] = K_w/[H^+] \qquad (28)$$

$$[HCO3^-] = \frac{TA+[H^+]-[OH^-]}{(1+2\times K_2/[H^+])} \qquad (29)$$

$$[CO3^{2-}] = \frac{TA+[H^+]-[OH^-]}{2\times(1+[H^+]/2K_2)} \qquad (30)$$

$$[CO2] = \frac{[H^+]}{K_1} \times \frac{TA+[H^+]-[OH^-]}{(1+2\times K_2/[H^+])} \qquad (31)$$

The TA in equivalents per litre is equal to:

$$TA = [HCO_3^-] + 2[CO_3^{2-}] + [OH^-] - [H^+] \qquad (32)$$

and TC is equal to:

$$TC = [HCO_3^-] + [CO_3^{2-}] + [CO_2] \tag{33}$$

In this work, since the interest is to estimate the fouling in the MSF tubes, thus no evaporation of water or escape of CO_2 occur here. Both TA and TC are consumed when $CaCO_3$ precipitates [8]. Thus, the values of TA and TC in the following stages can be calculated according to the following equations:

$$TA_{(j+1)} = TA_{(j)} - CaCO_{3(j)} - {}^1\!/_2\, Mg(OH)_{2(j)} \tag{34}$$

$$TC_{(j+1)} = TC_{(j)} - CaCO_{3(j)} \tag{35}$$

3.2 Removal rate

Increasing the fouling thickness can reduce the tube cross-sectional area and gradually increase the pressure drop and in some cases, this can cause a complete block of the tubes. With time, due to the increase of the shear force, the accumulated scale becomes weak and more fragile and parts of the deposit rate starts to breakdown. This mechanism is called removal rate and it was assumed to be proportional to the wall shear stress of the flow and inversely proportional to the layer's shear strength [39]. The removal rate can be calculated using the following equation:

$$\frac{dm_r}{dt} = k_{rem}\frac{\tau_f}{\sigma_f}\rho_f\left(\frac{\mu_w g}{\rho_w}\right)^{1/3} \tag{36}$$

Where k_{rem} is a constant related to the removal rate, σ_f is the shear strength of the fouling layer, ρ_f is the density of the deposit and g is the gravitational acceleration.

Shear strength can be calculated using the following equation [39]:

$$\sigma_f = K.\frac{P}{N.x_f(1+\delta\Delta T).d_p} \tag{37}$$

Where P is the intercrystalline adhesion force, K is a constant, N is the number of defects in fouling layer, ΔT is the temperature difference within the fouling layer, δ is the linear expansion coefficient, x_f is the layer thickness and d_p is the crystal size.

Substituting Equations (37) into Equation (36) results in the following equation:

$$\frac{dm_r}{dt} = \frac{k_{rem}.N.x_f(1+\delta\Delta T).dp.\tau_f}{k.P}.\rho_f.\left(\frac{\mu_w g}{\rho_w}\right)^{1/3} \tag{38}$$

The term $(k.P/k_{rem}.N)$ is calculated based on Krause's suggestion according to the following equation [22]

$$\frac{k.P}{k_{rem}.N} = 83.2 \times v^{0.54} \tag{39}$$

And it follows

$$\frac{dm_r}{dt} = \frac{x_f(1+\delta\Delta T).dp.\tau_f}{83.2 \times v^{0.54}} \cdot \rho_f \cdot \left(\frac{\mu_w g}{\rho_w}\right)^{1/3} \tag{40}$$

3.3 Fouling resistance

The net mass deposit (dm_f/dt) in Equation (1) can be determined as a function of the mean thickness (x_f) and the density (ρ_f) of the crystal layer.

$$\frac{dm_f}{dt} = \rho_f \times \frac{dx_f}{dt} \tag{41}$$

Also, at any location of the heat transfer area, the fouling thermal resistance (R_f) can be calculated as a function of the mean thickness (x_f) and conductivity (λ_f) of the crystal layer.

$$\frac{dR_f}{dt} = \frac{1}{\lambda_f} \times \frac{dx_f}{dt} \tag{42}$$

Thus, combining Equations (1), (41) and (42), the fouling thermal resistance rate can be calculated as a function of the deposit and removal rate.

$$\frac{dR_f}{dt} = \frac{1}{\lambda_f \times \rho_f} \times \left[\frac{d_{md}}{dt} - \frac{d_{mr}}{dt}\right] \tag{43}$$

Equation (43) has been implemented in similar or different form by many researchers to predict the fouling behaviour in heated surfaces. However, over or under estimation of the parameters can lead to different shape of the fouling factor curve. Mwaba et al. [24] reported that some of the studies presented fouling curve to be of an 'S' shape, depending on the roughness of the surface and concentration of the ions. The 'S' shape can be obtained if the nucleation period is considered in the development of fouling. The period of nucleation may vary from seconds to hours depending on the temperature, concentration and the velocity [7]. However, Figure 7 presented by Hamed and Al-Otaibi [29] shows the fouling behaviour in MSF brine heater and the shape of the curve does not look like 'S' shape. This can be attributed to the fact that the nucleation period is very short and thus it can hardly be seen. Although Figure 7 was obtained at MSF brine velocity higher than 1.5 m/s, Brahim et al. [22] and Zhang et al. [27] results were consistent with Hamed and Al-Otaibi's results though their flow velocity was as low as 0.2 m/s. Moreover, though the removal rate was included in their model, their fouling curve looked linear and no major effect of the removal rate on the shape of the fouling curve was observed. This can be attributed to the low velocity of the fluid or the shortness of the experimental time.
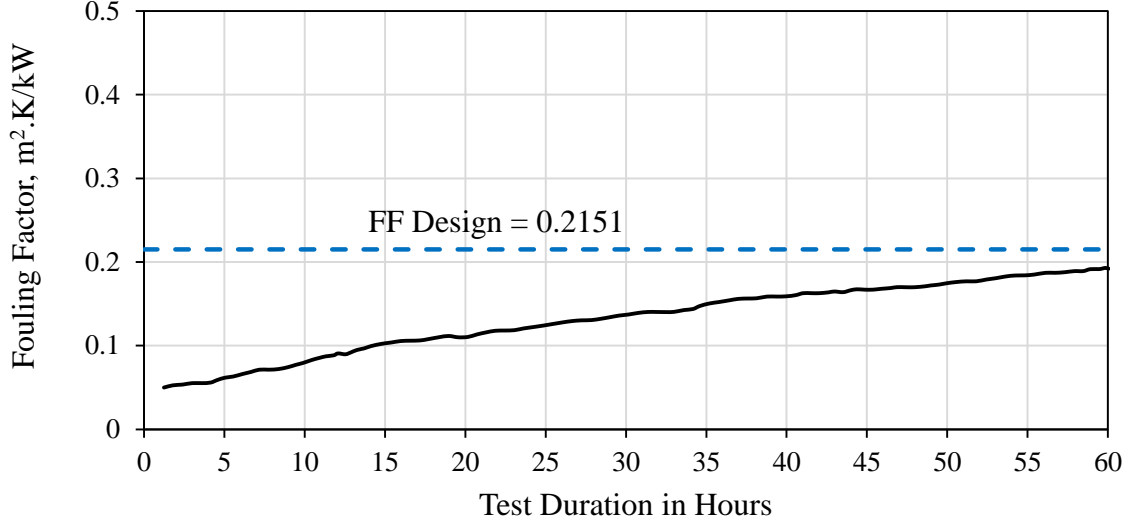
Figure 7: Brine heater fouling factor at TBT 119 °C without antiscalant [29].

While the flow velocity is well known as an important factor in removal rate, it also affects the deposit rate. The fouling rate increase in low-velocity regions, especially where the velocity drops suddenly [46]. Paakkonen et al. [41] mentioned that the deposit rate increases as the residence time of the fluid increases (Low velocity). In MSF evaporated stages and heat exchangers in general, the evaporated tubes are connected to each other by water boxes where the velocity drops suddenly and thus more fouling is expected at the outlet tubes and on the shell side of the water boxes. In fact, Elmoudir et al. [47] found out that the scale was concentrated in hot outlet location of the stages and more than 50% of the outlet tubes were blocked (Figure 8). They assumed that 50% of the deposit rate was accumulated at the water boxes and does not affect the overall heat transfer surface. This amount of the deposit at the outlet of the tubes could be as result of the removed particles from the tubes that stick again at the outlet of the tubes and in the water boxes due to the sudden decrease in the velocity.

To calculate the density of the fouling layer, Zhang et al. [27] approach is adopted in this work. Zhang and his co-workers assumed that the fouling layer is a porous material with a porosity of ω. the fouling layer density correlation can be written as following:

$$\rho_f = \omega \times \rho_{air} + (1 - \omega) \times \rho_{solid} \tag{44}$$

Where the ρ_{solid} is the density of the compact solid.

Since the assumed porous material is immersed in the bulk, the conductivity of the fouling layer is estimated based on Brahim et al. [22]'s correlation. Here, it is assumed to be the arithmetic average value of thermal conductivity of deposit/water system.
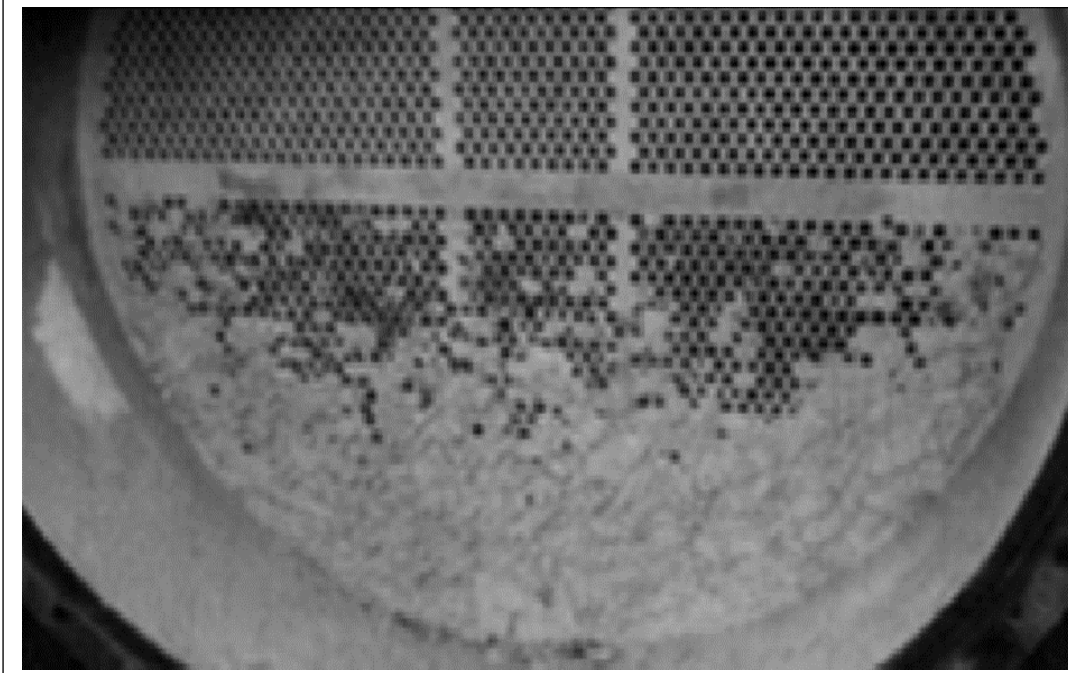
$$\lambda_f = \frac{\lambda_{f,I} + \lambda_{f,II}}{2} \tag{45}$$

where

$$\lambda_{f,I} = \omega.\lambda_{water} + (1 - \omega).\lambda_{solid} \tag{46}$$

$$\frac{1}{\lambda_{f,II}} = \frac{\omega}{\lambda_{water}} + (1 - \omega)/\lambda_{solid} \tag{47}$$

where λ_{water} is the conductivity of pore medium (water) and λ_{solid} is the thermal conductivity of compact solid.

Elmoudir et al (2008). Process modelling in desalination plant operations. Photo 1. Page 435. *Desalination,* vol. 222, pp. 431-440.

Figure 8: Fouling in brine heater after operation for a period at TBT = 115 $^{\circ}$C [47].

Finally, the fouling resistance can be introduced into the overal heat transfer coefficient equation as follows.

$$\frac{1}{U_o} = \left(\frac{d_o}{h_i d_i}\right) + \left(R_{f,i}\frac{d_o}{d_i}\right) + \left(\frac{d_o}{2k_t}\right) Ln\left(\frac{d_o}{d_i}\right) + R_{f,o} + \left(\frac{1}{h_o}\right) \tag{48}$$

Where d is the tube diameter in m, k_t is the tube material thermal conductivity in kW/m.K, h is the heat transfer coefficient in kW/m^2.K, and the subscripts o and i refer to the outer and inner tube surface respectively. While $R_{f,i}$ is the fouling resistance inside the tubes in m^2.K/kW, the outer fouling resistance, $R_{f,o}$, is kept constant in this work.

4. Results and Discussion

The dynamic model of fouling was implemented using gPROMS model builder and then it is incorporated into the whole MSF dynamic model of Alsadaie and Mujtaba [48]. The whole simulation of MSF process is run for an adequate time with and without antiscalant to check the deposit rate and the fouling rate. The chemical analysis of seawater that used in this work is presented in Table 1.

The pre-exponential constant, k_{r0}, and the activation energy, Ea, are calculated experimentally from the deposit rate and saturation index by the Arrhenius equation [36]. There are no specific values for these parameters to be adopted for carbonate or magnesium systems. Paakkonen et al. [49] mentioned that these parameters vary largely depending on the velocity, and thus they conclude that more factors should be considered to calculate these parameters. However, for diffusion controlled process, Andritsos et al. [35] reported a weak effect of the fluid velocity on the activation energy of carbonate system. Paakkonen et al. [41] found out that the effect of activation energy is much stronger than the effect of pre-exponential constant. In the present work, and due to the lack of experimental data for fouling in MSF process, values for k_{r0} and Ea for calcium carbonate were assumed to be ($k_{r0} = 1.8x10^{10}$ $m^4/kg.s$ and $Ea= 68.210$ kJ/mol). Precipitation of magnesium hydroxide has less attention than calcium carbonate and the number of studies of the precipitation of magnesium hydroxide are considerably less than that for calcium carbonate. However, Shams El Din and Mohamed [50] reported that the amount of calcium carbonate in the water boxes of the first stages was approximately 7 times more than magnesium hydroxide. Thus, the values of k_{r0} and Ea for hydroxide magnesium precipitation have been estimated to be ($k_{r0} = 6.4x10^{18}$ $m^4/kg.s$ and $Ea= 120$ kJ/mol) to match the ratio of calcium carbonate precipitation to magnesium hydroxide precipitation.

Table 1: Chemical analysis of the seawater entering the heat rejection section

Parameters	Unit	Brine recycle to HRS
pH		8.2
Total alkalinity	mg/L as CaCO$_3$	106
Sulphate	mg/L	6081
Calcium	mg/L	894
Magnesium	mg/L	2886

(Source: Hamed and Al-Otaibi [29])

4.1 Running the MSF simulation without antiscalant.

Running the MSF simulation model with the predicted fouling factor and without antiscalant for long time may lead to infeasible solution. This happened due to the fact that overall heat transfer coefficient and flow velocity could reach unacceptable values which can make the MSF profess infeasible to operate. Thus, the simulation was run for a certain time to avoid unrealistic fouling.

As mentioned before (Section 2, Figure 3), the recycle brine is pumped from the last stage in HRJ (Stage 24) into the last stage of the HRS (Stage 21) at around 40 °C where it is heated gradually to around 112 °C at the outlet from stage 1 before the water enters the brine heater for further heating. . Due to the increase in surface temperature and decrease of the saturation concentration from stage to stage, the deposit of both CaCO$_3$ and Mg(OH)$_2$ increased. The deposit rates of calcium carbonate and magnesium hydroxide per unit area are shown in Figure 9. As it can be seen, the calcium carbonate starts to precipitate at low temperature while magnesium hydroxide starts to precipitate at higher temperature. At low temperature

stages, the OH ions are too low to cause any precipitation of magnesium hydroxide. However, as the recycle brine flows through the stages and its temperature increases, its solubility is reached resulting in deposition of magnesium hydroxide. At saturated brine of calcium carbonate and magnesium hydroxide, the priority of crystallization depends on the Ca/Mg or CO_3/OH ratio. Dooly and Glater [51] reported that the precipitation of calcium carbonate will be favoured by an increase in the ratio of Ca/Mg or CO_3/OH. Here, in this work, the participation of calcium carbonate in stages from 21 to nearly stage 5 leads to reduction of the Ca/Mg ratio and thus precipitation of magnesium hydroxide becomes more favoured from stage 5 to the first stage.

An actual data is hard to obtain form real plants due to the difficulties of having deposit sample from MSF tubes. However, Shams El Din and Mohamed [50] conducted very rigorous analysis of the collected samples from flash chambers pools and water boxes from two different MSF plants. In their analysis, they reported that the deposit mass of calcium carbonate in the first three water boxes was approximately 7 times more than magnesium hydroxide. The $Mg(OH)_2$ starts to precipitate from stage 9 where the surface temperature is around 82 ^{o}C, which is consistent with the observations of Wildebrand et al. [52] when they spotted a thin layer of $Mg(OH)_2$ crystal at 80 ^{o}C.

Figure 9 also shows that while there is a decrease of the precipitation of calcium carbonate in the first few stages, there is a slight increase in the middle stages. This can be explained by the increase in the vapour and brine temperatures in the middle flash chambers. As it can be seen in Figure 10, the surface temperature of the first few stages decreases with time due to the fouling whereas the temperature in the middle stages increases. While there is a reduction in the surface temperature due to the fouling, the vapour temperature inside the flash chambers increases leading to increase in the heat transfer flux and as a result, more deposition is expected in the middle stages. This increase in the $CaCO_3$ deposition in the middle stages may cause reduction in the Ca concentration and thus the deposition of calcium carbonate in the first few stages decrease and the deposition of magnesium hydroxide becomes more favourable over calcium carbonate. However, in long run, the deposition of calcium carbonate and magnesium hydroxide decrease due to the decrease in the surface temperature. Moreover, since the carbon dioxide (CO_2) is formed alongside with the formation of $CaCO_3$, then the release rate of CO_2 can be good indicator of the deposit rate of calcium carbonate. As it shown in Figure 10, the concentration of CO_2 increases as calcium carbonate is produced and then starts to decrease with the decrease in the deposition of calcium carbonate.
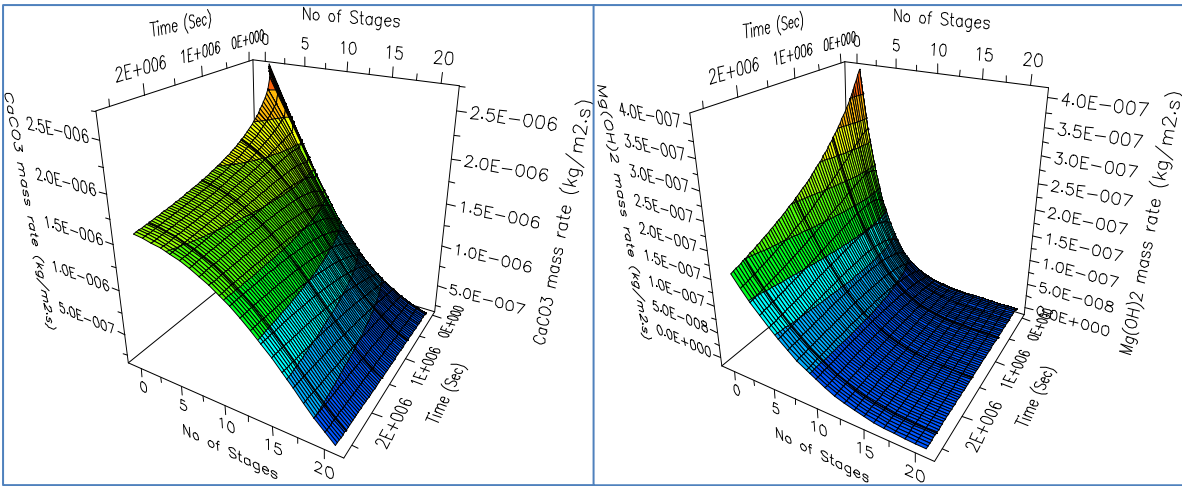
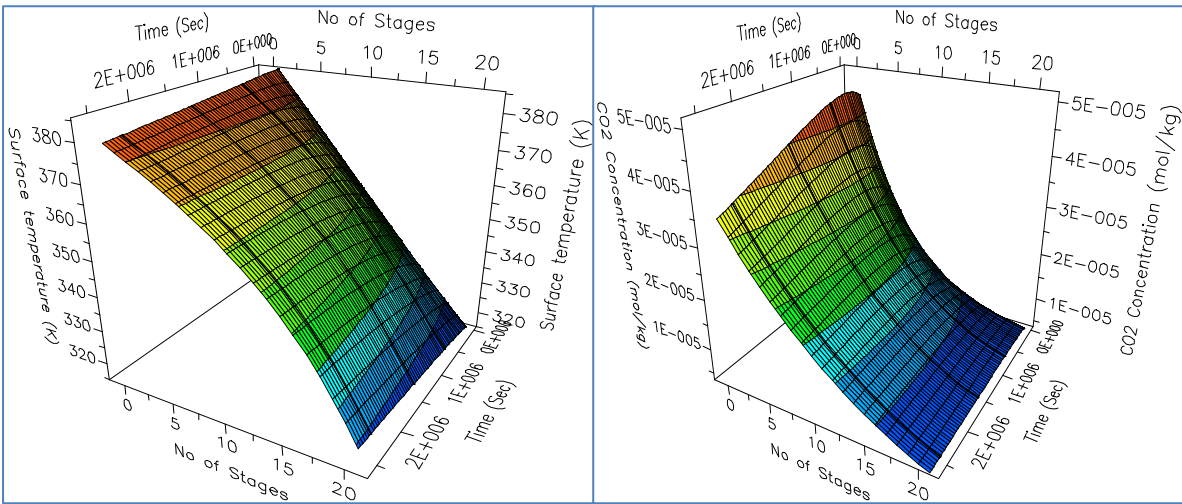Figure 9: Calcium carbonate mass rate (left) and magnesium hydroxide mass rate (right).

Figure 10: Surface temperature profile (left) and CO_2 concentration profile (right)

Due to the lack of information of fouling without antiscalant, the fouling in the first stage, as it has the highest temperature (around 112 ^{o}C), is compared to the brine heater fouling without antiscalant presented by Hamed and Al-Otaibi [29] in Figure 7. The results presented in Figure 11 show slight difference between this model's results and the extrapolated results presented by Hamed and Al-Otaibi [29]. This can be explained by the temperature difference between the brine heater and the first stage. Hamed and Al-Otaibi results were obtained in brine heater (119 ^{o}C) while this results was for the first stage (112 ^{o}C) in the MSF plant. Figure 12 shows the fouling profile per stages. Though the deposition rate decreases in the first few stages and increases in the middle stages, the Figure 12 shows high fouling in the first stage and decrease towards the number of stages as the temperature decreases.
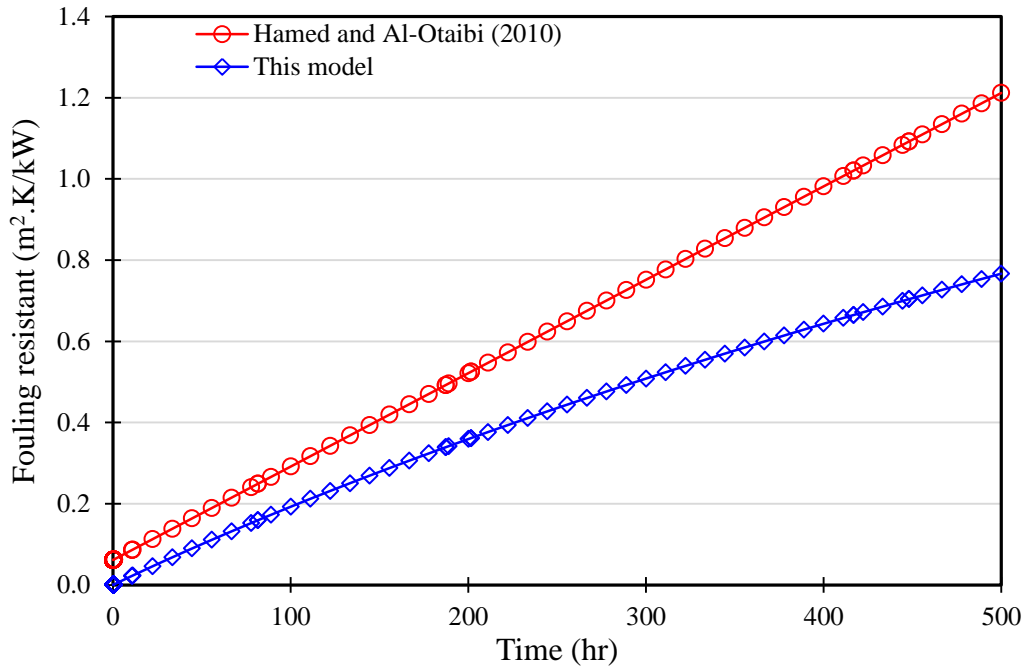
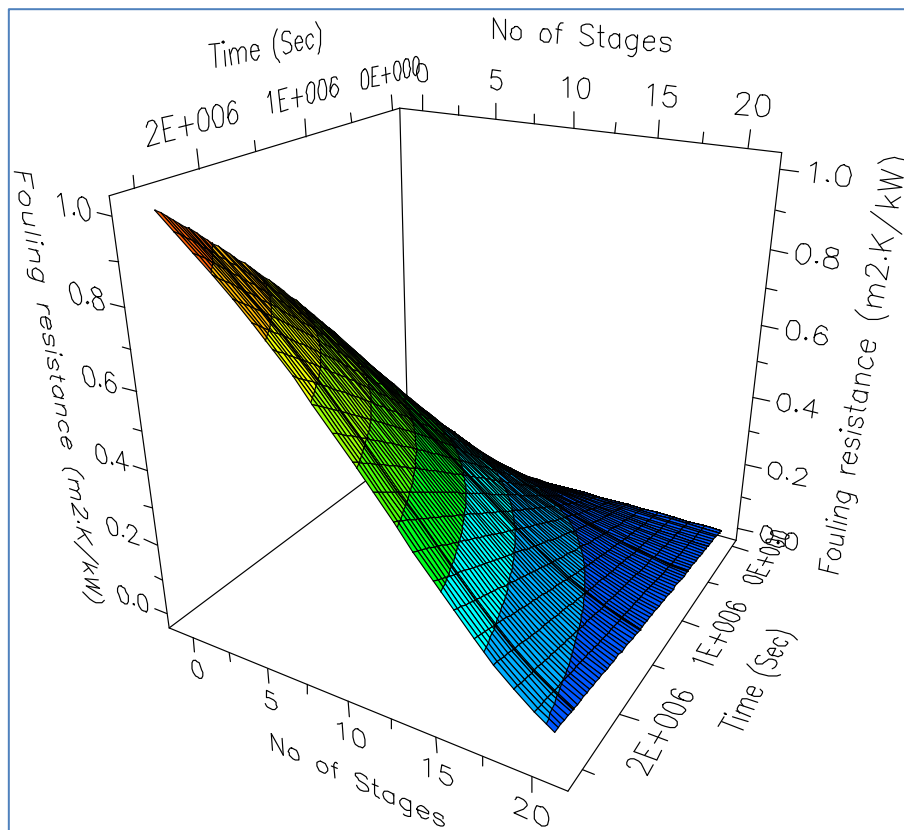Figure 11: Predicted fouling resistance as a function of time.

Figure 12: Fouling resistance profile as function of the number of stages and time

Considering the first stage as it has the highest temperature, Figure 13 shows the total deposit rate per unit time together with the net deposit rate and the removal rate. The total deposit rate decreases with time due to the decrease in the surface temperature of the fouling layer.

Alongside this decrease in the deposition rate, the removal rate increases due to the growth of the fouling layer and consequently the velocity of the brine increases causing more particles to be removed. With the increase of the removal rate, the net deposit rate becomes less than the total deposit rate by the difference of the total deposit rate and the removal rate. The rapid or slow decrease in the net deposit rate depends on the removal rate which is strongly depends on the fouling layer thickness and brine velocity inside the tubes. Figure 13 also shows that the deposit rate is nonlinear and it appears to approach steady state with time as there is enhancement in the heat transfer. Brahim et al [22] reported that the supersaturation at the interface is reduced due to the increase in the velocity and thus the heat transfer is improved. Moreover, the reduction in the recycle brine salinity can also considered to be another parameter to slow the decrease of the deposit rate. According to equation (20), the solubility product of calcium carbonate increases with the decrease in the temperature resulting in decrease in the deposit rate. However, Mucci [53] reported that the solubility product decreases with the decrease in the salinity resulting in increase in the deposit rate. Thus, considering only the temperature effect is not very accurate to predict the deposit rate. Due to the decrease in the recycle brine salinity, the solubility concentration of calcium carbonate does not increase the deposit rate but rather it slows down the decrease caused by the drop in the temperature.
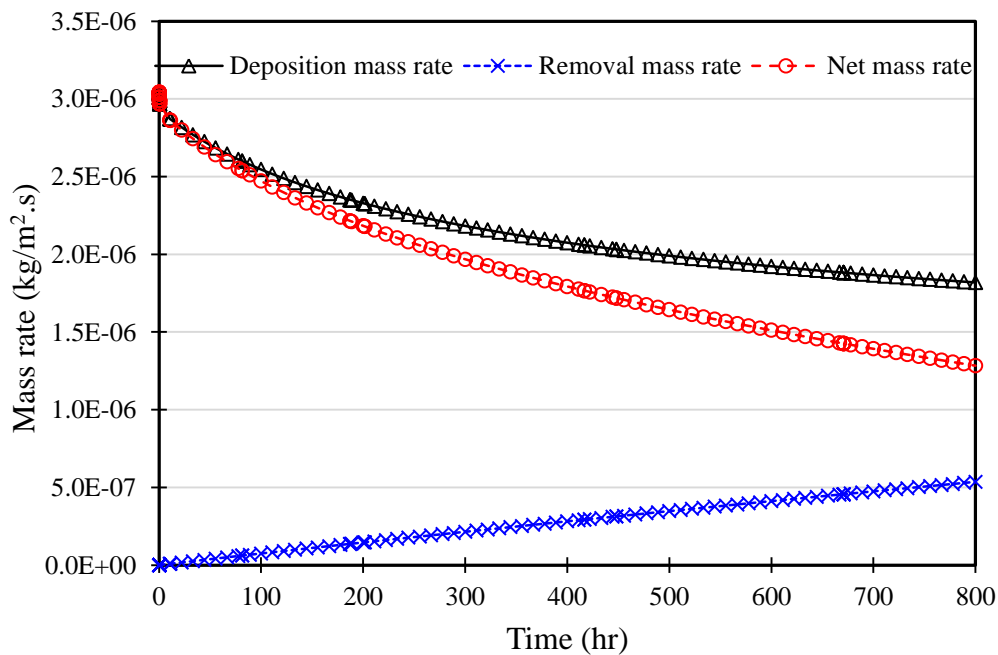

Figure 13: Deposit rate together with removal rate and net rate.

4.1.1 Effect of flow velocity.

In many studies, the effect of the flow velocity on fouling varies based on the controlled mechanism of the fouling. Though Helalizadeh et al. [40] reported a decrease in the mass deposit rate with increase in the velocity during convection heat transfer and sub-cooled flow boiling experiment, Najibi et al. [7], Helalizadeh et al. [11] and Peyghambarzadeh et al. [54] reported that the fouling resistance increases with increase of the flow velocity. They

explained that the diffusion mechanism has some control on the fouling resistance at certain velocities and then when the velocity increased further, the fouling became completely reaction control and the deposit rate is flow velocity independent. It is important to mention that the previous three studies were conducted to predict the fouling rate under subcooled flow boiling. Moreover, Andritsos et al. [35], who adopted diffusion mechanism controlled process, reported increase in the deposit rate with increase in the fluid velocity. They concluded that this trend was an indication of the diffusion controlled mechanism. Paakkonen et al [41], however, showed a decrease in the mass deposition rate of calcium carbonate with an increase in the flow velocity.

In the presence of fouling, though at constant volumetric flow rate, the flow velocity inside the MSF tubes varies with time due the variation in the cross sectional area. However, different values of flow velocity can be set to observe its effect clearly. Hence, different values of flow velocity at the start of every run can be obtained by adjusting the recycle volumetric flow rate. In the present work, four different values of the recycle flow rate (3.25, 3.5, 3.75 and 4.0 m^3/s) were selected to obtain four different velocity values. Increasing the velocity by increasing the volumetric flow rate by 0.25 m^3/s results in a very slight increase in the deposit rate of calcium carbonate as shown in Figure 14. However, further increase in the velocity results in decrease in the deposit rate of calcium carbonate. Though Brahim et al [22] reported that the heat transfer can be improved due to the increase in the velocity, Paakkonen et al [41] pointed out that reducing the resident time of the fluid at the surface may decrease the probability of the fouling material to stick to the surface. As it can be seen in Figure 15, the heat transfer was slightly improved with the increase in the velocity. Further increase in the volumetric flow rate to its maximum value (4.0 m^3/s) leads to more reduction in the deposit rate of calcium carbonate though the heat transfer is improved. However, the variation in the salinity of seawater can play an important role in the fouling behaviour in MSF process. Increasing the recycle brine velocity can improve the heat transfer and thus increase the salinity of the recycle brine. This can lead to decrease in the activity coefficients of the seawater ions and consequently increase the solubility product of calcium carbonate and magnesium hydroxide. Thus, the concentration driving force decrease resulting in decrease in the deposit rate.

Hence, different results can be obtained if the salinity is assumed to be constant. Here, figure 16 shows the deposition rate of calcium carbonate with different velocities and at constant salinity. As it can be seen, the deposit rate of calcium carbonate increases with the increase in the velocity. However, this increase in the deposit rate is limited to certain velocities and with further increase in the velocity, it becomes temperature dependent and the velocity has no effect.
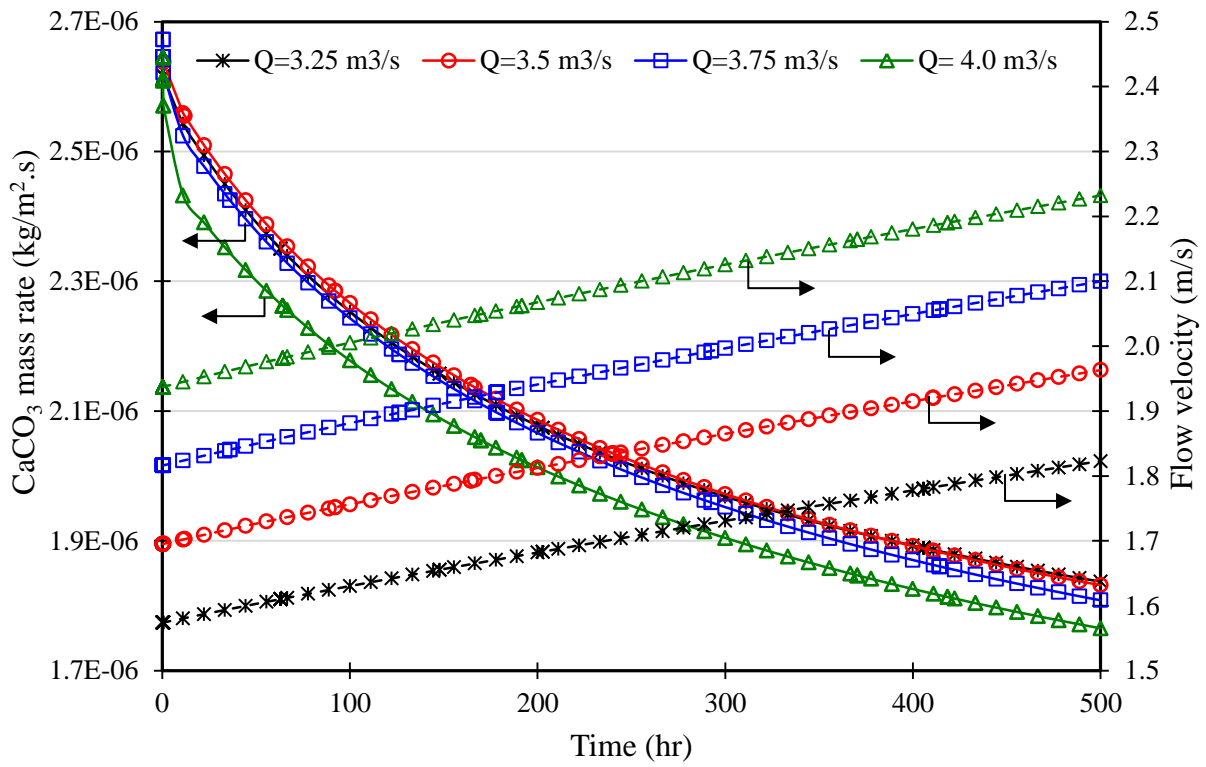
Figure 14: Effect of the flow velocity on the deposition rate of CaCO$_3$ (First Stage)
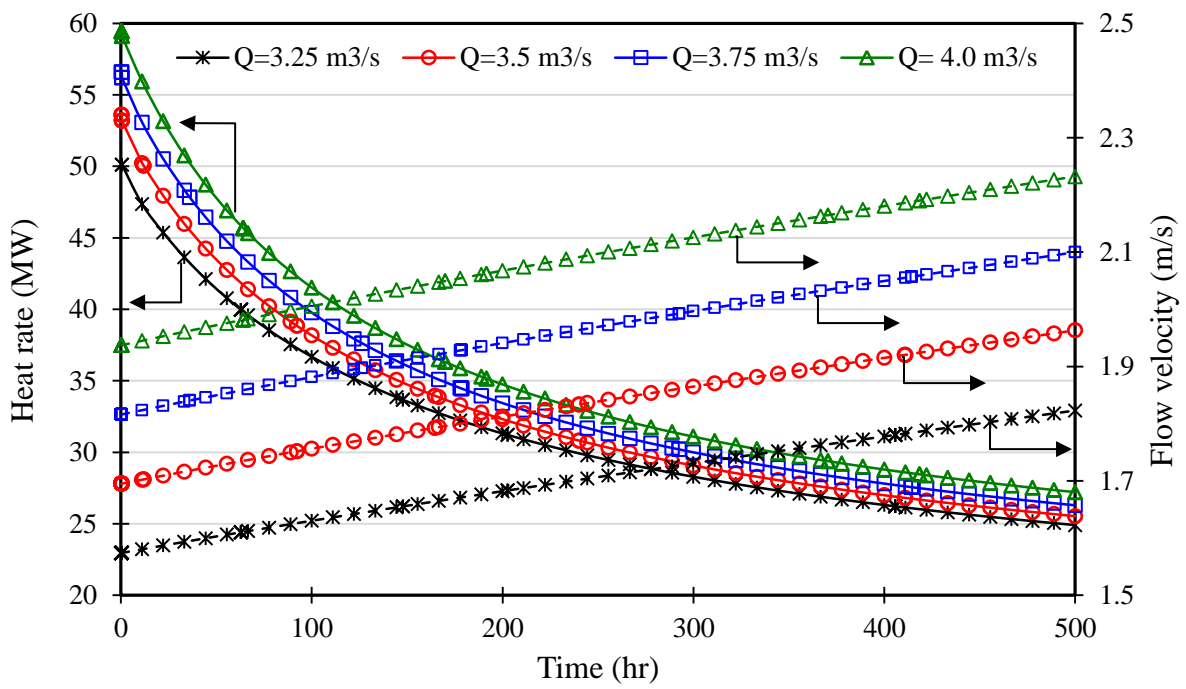
Figure 15: Effect of the flow velocity on the heat transfer rate (First Stage)
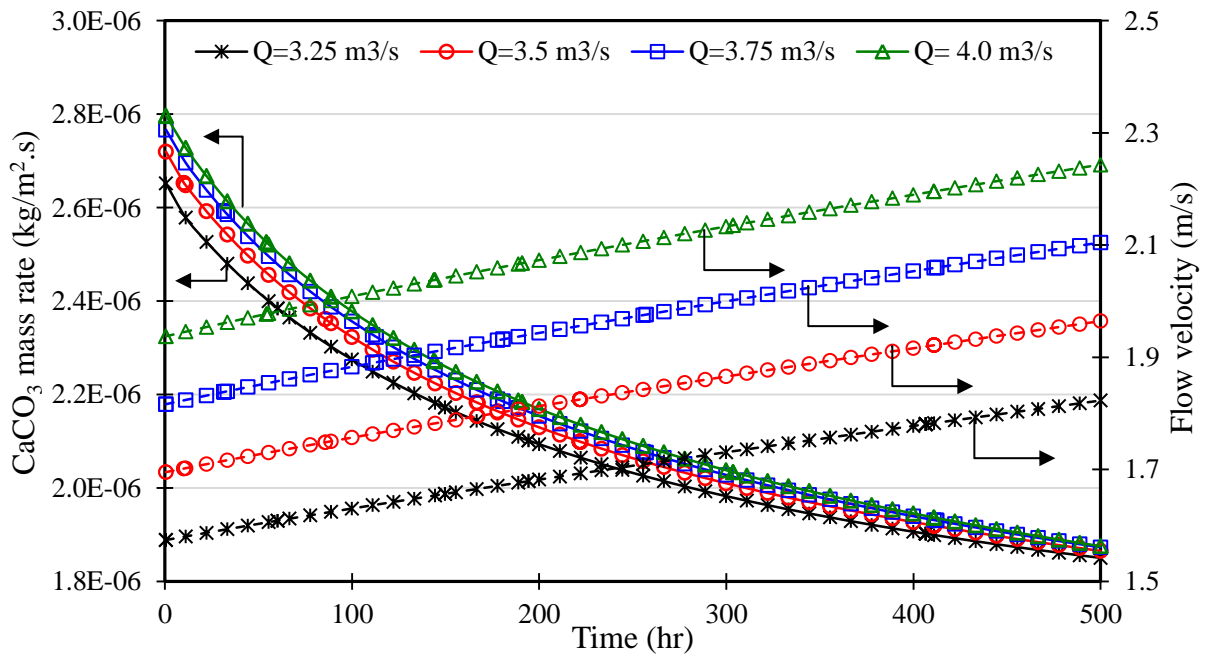

Figure 16: Effect of the flow velocity on the deposition rate of $CaCO_3$ at constant salinity (First Stage)

In the case of magnesium hydroxide, however, the deposit rate increase with the increase in the flow velocity. Due to low solubility product of magnesium hydroxide, the activity coefficients of magnesium and hydroxide ions have no great effect on magnesium hydroxide precipitation. Figure 17 shows that the increase in the magnesium hydroxide follow the same pattern as the heat transfer rate and thus it is believed here that the precipitation of magnesium hydroxide is temperature dependent and the velocity has no direct effect.
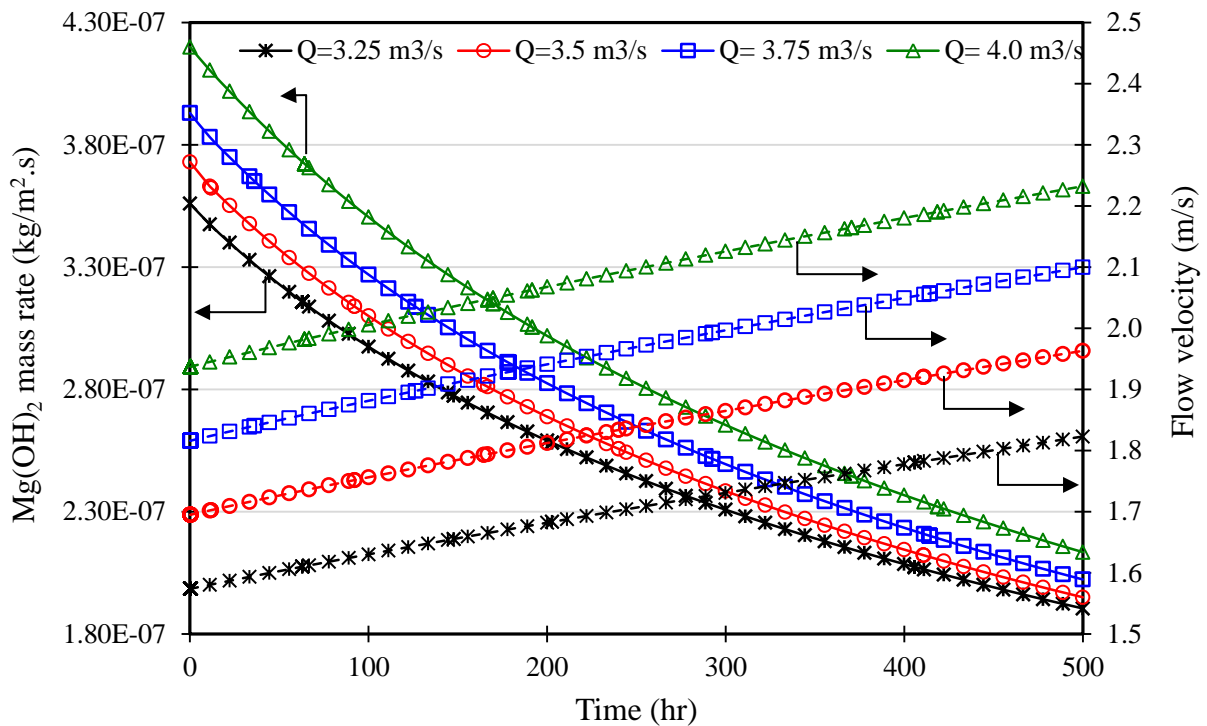
Figure 17: Effect of the flow velocity on the deposition rate of Mg(OH)$_2$ (First Stage)

However, despite the increase in the heat transfer rate and the deposition rate of magnesium hydroxide with the increase in the flow velocity and also slight increase and then decrease of the deposition of calcium carbonate, at constant volumetric flow rate, both the deposition of calcium carbonate and magnesium hydroxide and also the heat transfer rate decrease with the increase in the velocity. This can be explained by the increase in the fouling layer thickness which affects the heat transfer rate and consequently affects the deposition rate of calcium carbonate and magnesium hydroxide.

While the deposit rate has positive effect on the fouling, the removal rate, on the other side, has reverse effect on the fouling mechanism. The removal rate depends on the thickness of the fouling layer and strongly on the flow velocity of the brine. Figure 18 shows the effect of the velocity on the fouling resistance and removal rate in the first stage of the MSF plant. Due to the increase in the thickness of the fouling layer and the velocity of the brine, the effect of the removal rate increases. As it can be seen from figure 18, the effect of the removal rate on the fouling can be observed clearly after long run. Thus, high velocity can help to decrease the fouling rate by increasing the removal rate.
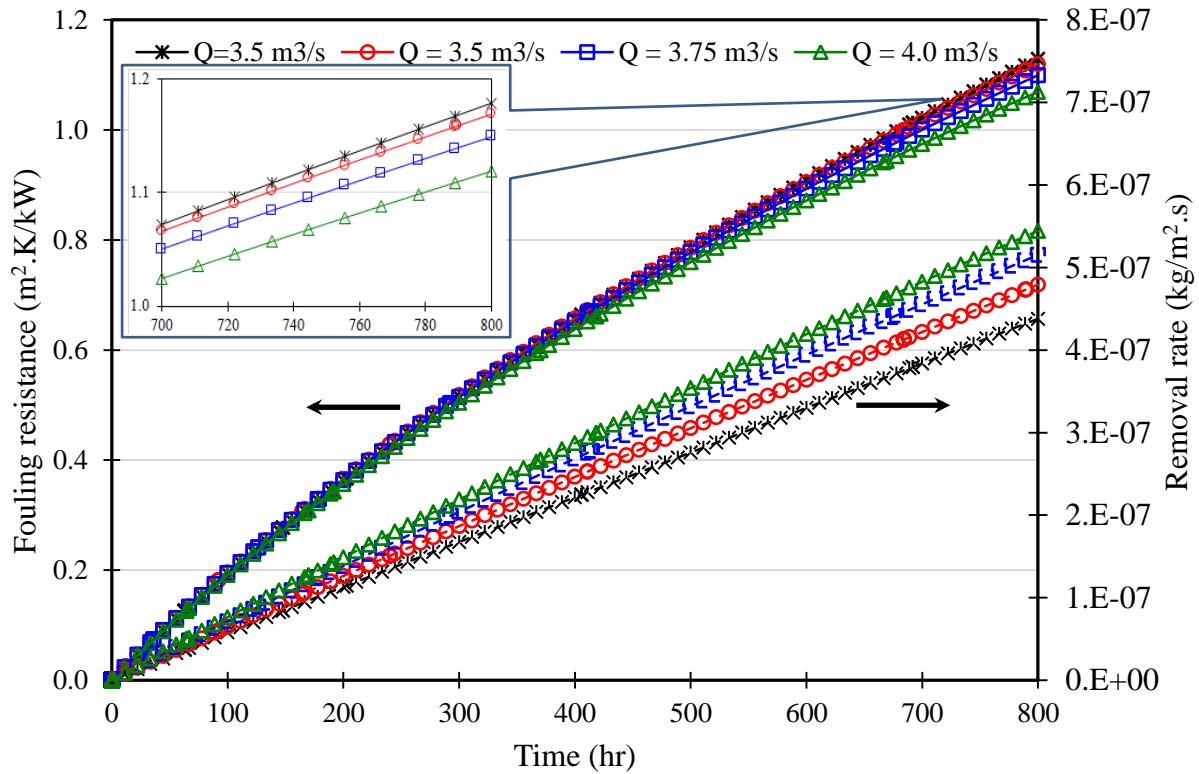
Figure 18: Effect of the flow velocity on the fouling resistance and removal rate (First Stage)

Though increasing the the flow velocity results in decrease in the fouling with time, in MSF process, increasing the velocity could affect the efficiency of the plant. The efficicnecy of MSF process is estimated by the performance ratio (PR) which can be defined as the amound of produced distillate per 1 kg of heated steam in the brine heater.

Helal et al. [55] and Abdul-Wahab et al. [56] reported that the main variables that affect the performance of the plant were the TBT and the brine recycle flow rate. Increasing one of these variables leads to increase the performance ratio and distillate product. Increasing the brine recycle flow rate may increase the distillate, however, increase it over the design point would inevitably affect the overall MSF plant cost [57]. Figure 19 shows the performance ratio at different velocities. As it is expected, the performance ratio decreases with increasing the velocity though increasing the velocity decreases the fouling rate and enhance the heat transfer rate. This reduction in the performance ratio can be explained by the increase in the amount of steam that used to heat the recycle brinere [58]. Thus, optimum value of the brine recycle flow rate can be obtained to maximize the performance ratio and distillate product.
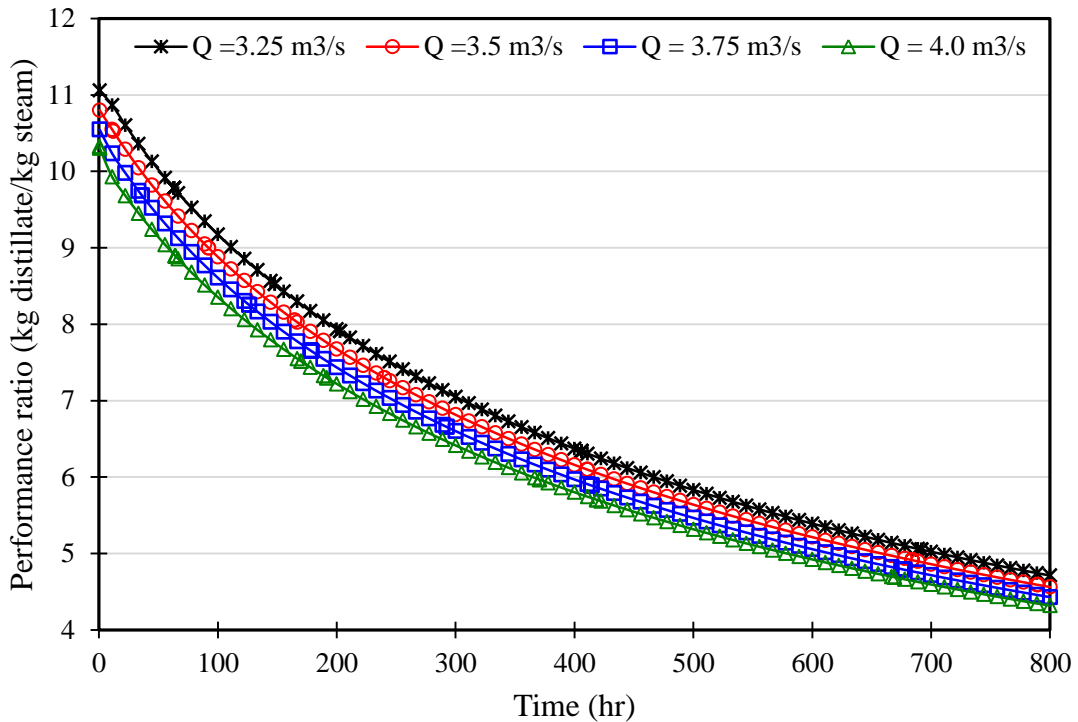
Figure 19: Effect of the flow velocity on the plant performance ratio in the presnece of fouling.

4.1.2 Effect of surface temperature.

Since the MSF stages operate at different temperatures, its highest value in the first stage and decreases gradually from stage to stage due to gradual pressure drop. The effect of the surface temperature can be seen in Figure 12 as fouling resistance was plotted against the number of stages. Due to the decrease in the inner surface temperature from the first stage towards the last stage, the fouling resistance rate decreases. However, different MSF plants opeartes at different TBT based on the different parameters such as seawater salinity, seawater temperature and specific design of the MSF plant. Hence, in this part and to see clearly the effect of TBT on the fouling behaviour, theTop Brine Temperature (TBT) is varied between 90 ^{o}C and 119 ^{o}C for four intervals (90, 100, 110 and 119 ^{o}C). This variation leads to the inner surface temperature in the first stage to be varied between 84 ^{o}C and 112 ^{o}C. Figure 20 presents the mass deposit rate of calcium carbonate and magnesium hydroxide at 4 different TBT values for a period of 800 hours. Indeed, the mass deposit rate of both components increases with increasing the TBT. However, with the increase in the temperature, the increase rate of calcium carbonate in the first stage slows compared to the increase in the deposit rate of magnesium hydroxide. This can be explained by the reduction of calcium and carbonate ions in the first stages due to the increase in the calcium carbonate in the middle stages. As mentioned earlier (Section 6.1), increasing the temperature causes increase the temperature of the flash chambers in the middle stages and hence it results in more deposit in the middle stages and reduction in the calcium and carbonates ion in the first stages. Figure 21 shows the deposit rate of calcium carbonate per stage for 4 different TBT values after a peroid of 300 hours. Increasing the temperature shows an increase in the

deposit rate of calcium carbonate in the middle stages. This increase in the deposit rate in the middle stage affects the concentartion of calcium and carbonate in the first few stages.

The reduction in calcium and carbonate ions leads to decrease in the Ca/Mg and CO_3/OH ratio as reported earlier and thus, the deposition of magnesium hydoxide become more favourable. This can be seen clearly (Figure 20) as the deposit rate of calcium carbonate slow down, the deposit rate of magnesium hydroxide increases rapidly with the increase in the temperture.
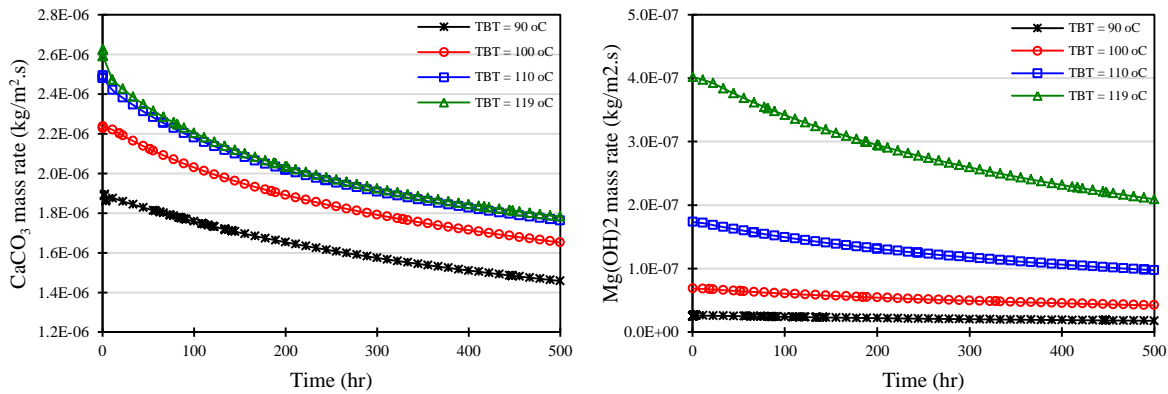
Figure 20: Effect of the surface temperature on the deposition rate of (left) calcium carbonate and (right) magnesium hydroxide (First Stage).
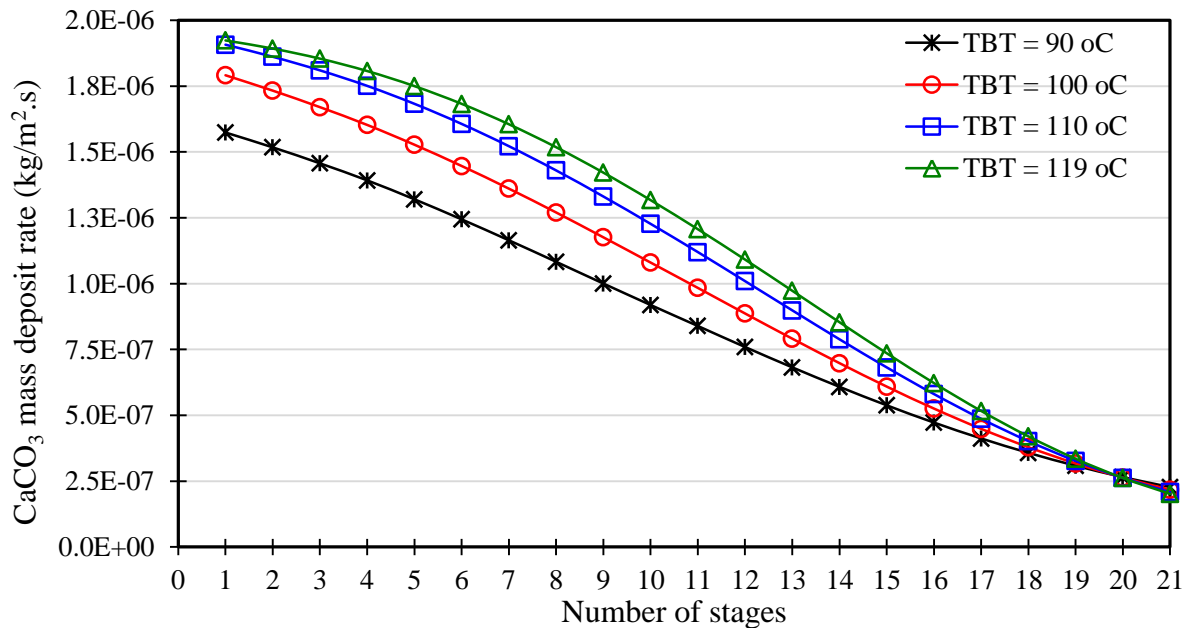
Figure 21: Deposit rate of calcium carbonate per stages after 300 hours of operation for 4 different TBT values.

4.2 Running the MSF simulation with antiscalant.

The MSF plants require scale prevention process to reduce the concentration of bicarbonate by using one of the commercial antiscalants alongwith sponge ball cleaning to reduce the

thickness of deposit layer of the fouling. The dosages rate of the antiscalants and the frequent use of ball cleaning depend on the hardeness of the seawater and the design of the MSF plants. Based on linear behaviour of the fouling, Hamed et al. [59] estiamted a period of around 375 and 483 days for polycarboxylic and polymaleic acids, respectively before the fouling reach the design value. However, this period can vary between one plant to another depending on many parameters such as the type of the antiscalants, the dosing rate, tubes material and the operation conditions of the plant. For the removal process using antiscalant, Andritsos et al. [35] reported experimently that use of acidified water can disolve 95% of the deposit in three hours.

It is important to mention that the main focus of the work is to develop fouling dynamic model that predicts the precipitation process. However, to highlight the essential role that antiscalant plays in controlling the fouling deposition, it is important to show the reader the bahviour of the plant in response to the action of the antiscalant. Hence, in this work, the reduction of the deposit process is done mathematically by decreasing the desposition growth by manually increasing the removal rate once the thickness of the foulinge layer reaches the design value. This can be done using task feature in gPROMS modelbuilder. First, the software is allowed to run for peroid until the thickness of the fouling layer reachs the design factor, and then new value of one parameter that has great impcat on removal rate is altered as there is exteral force (example; sponge balls) increases the removal rate. The process of cleaning will continue until the thicness is reduced to an acceptibal thickness, and then the software runs again in romal fouling mode and so on. It is assumed that during the cleaning process, the total deposit rate is negligible. By doing this, the process will run over long time without allowing the fouling factor to reach the design value. Hamed et al. [59] mentioned that the fouling factor of the HRS remained at almost a constant value during the whole period of the test. Moreover, Shams El Din and Mohamed [50] reported the water boxes of one unit of the Umm Al-Nar desalination plant (Abu Dhabi, UAE) were never opened. Another unit were opened only for inspection and repair. This long period without shutdown the plant is a good indicator of the effective of ball cleaning and the use of antiscalants in controlling scale formation

The result of fouling in the first stage is compared to the heat recovery section (HRS) fouling with the use of polyphosphonate antiscalant that was presented by Hamed et al [59]. Figure 22 shows the fouling resistance for the first stage together with Hamed et al [59] result for the period of 2500 hours. As it can be seen, the fouling factor is under control to be less than the design value (0.12 m^2.K/kW) for HRS.
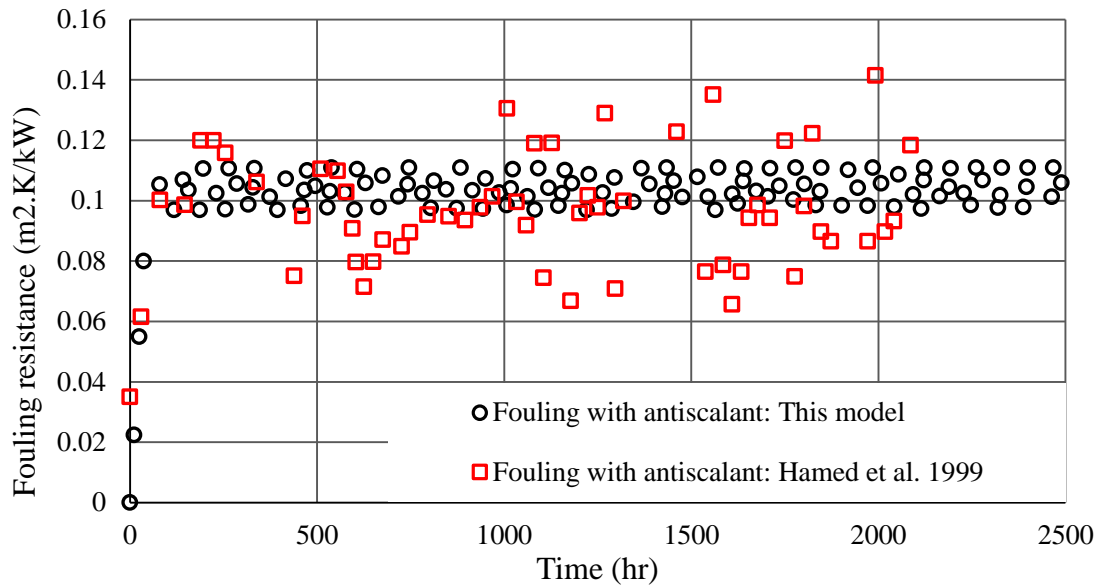
Figure 22: Estimated fouling resistance for the first stage in the presence of antiscalant

4.3 Performance ratio and plant capacity

Theoretically, by simulation, the plant performance ratio and its capacity are constant for the whole operation period. This is true since the operation parameters, like fouling design factor and the sea intake temperature, are fixed to be constant. However, in reality the story is completely different due to the variation of some parameters. Here in the present work, the model starts with clean tubes resulting in higher performance ratio and plant capacity. With time, the deposits accumulate inside the tubes and the fouling layer starts to build up leading to decrease in the overall heat transfer coefficient and consequently causing massive reduction in the performance ratio as preneted earlier in Figure 19. However, with the use of chemical antiscalant and ball sponge cleaning, the deterioration of thermal performance of MSF process can be avoided and the fouling can be controlled. Figure 23 presents the performance ratio of typical MSF plant at fixed fouling factor and varied fouling factor with antiscalant for a period of 4000 hours. As it can be seen, at constant fouling factor, the performance ratio is constant for the whole period. However, with the presence of fouling, the performance ratio is higher at the beginning when the tubes are clean and then starts to decrease with time because of increase in the fouling resistance. As soon as the cleaning process starts, the performance ratio decreases slowly and then remains at constant values above the design value.
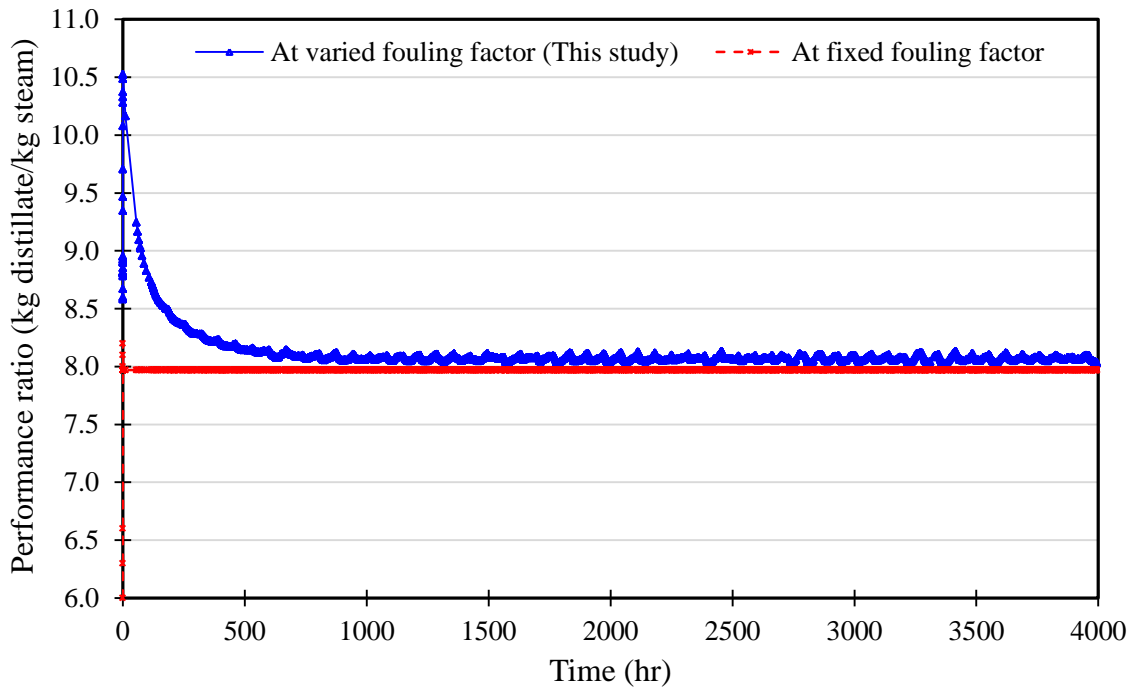
Figure 23: Performance ratio at fixed and calculated fouling factor

This effect can be seen in the plant capacity as well. The plant capacity, as it can be seen from Figure 24, follow the same behaviour of the performance ratio. When the fouling factor is assumed constant, the capacity value continues to be constant for the whole period while in the presence of fouling, the plant capacity at its highest value at the start of the process and then decline with time as the fouling resistance increase. The change in the plant capacity is not as much as the change in the performance ratio due to the fact that fouling resistance has great effect on the performance ratio and the total operation cost.

Figure 24: Plant capacity at fixed and calculated fouling factor with antiscalant.

5. Conclusions

In this work, deposition of calcium carbonate and magnesium hydroxide scale on a heated surface tubes of MSF process was studied through the use of dynamic fouling model integrated into MSF dynamic model. Brief description of the fouling phenomena was carried out to understand the fouling process in MSF plants. Very detailed review of the fouling models was 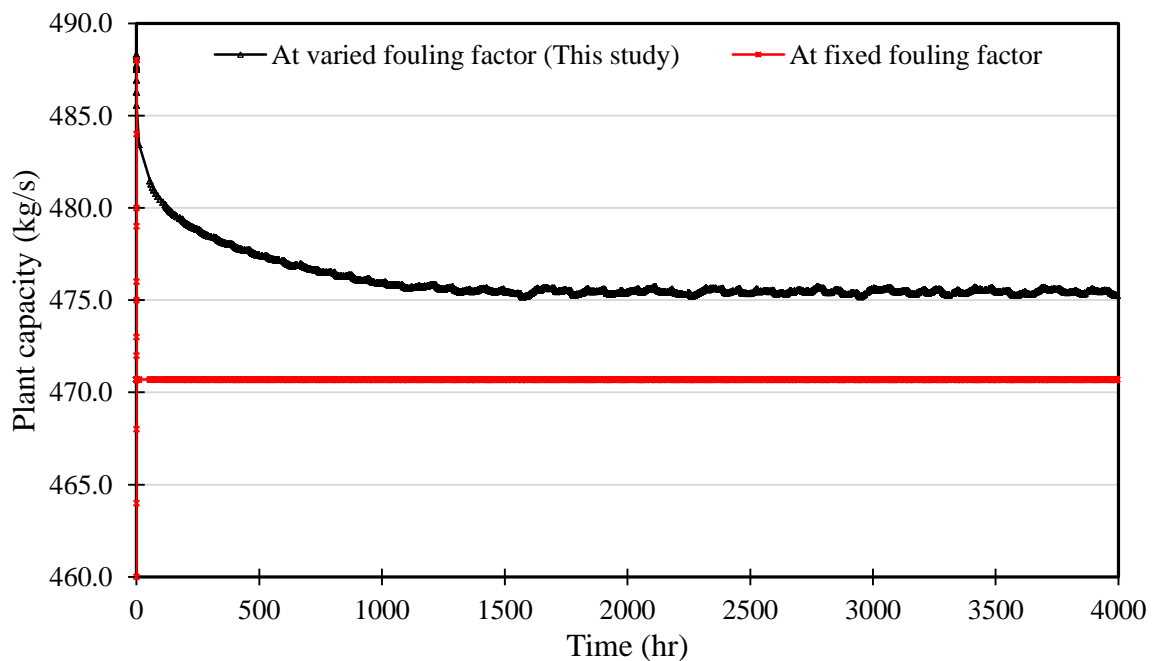conducted to obtain suitable model that can be implemented in MSF plants. The fouling model of calcium carbonate was modelled based on both diffusion and reaction mechanism. However, the deposition of magnesium hydroxide was modelled based on reaction mechanism due to the lack of diffusion data. The results of the proposed model were in good agreement with most of the recent studies.

The MSF simulation model was carried out under very harsh conditions of TBT around 119 ^{o}C. However, to investigate the effect of temperature and velocity, different runs were carried out at different TBT values and different volumetric flow. The results showed an obvious outcome that the potential of fouling increases with the increase in the stage temperature. The behaviour of the rate of increase of fouling was different from calcium carbonate and magnesium hydroxide. Unlike single heat exchanger unit, MSF plant is built up of number of single heat transfer stages connected in series and thus the increase in the temperature in the middle stages affected the concentration of Mg and Ca in the first few stages. Thus, due to the reduction in the Ca/Mg and CO_3/OH ratio, the increase of the deposition rate of magnesium hydoxide was higher than the increase of the deposition rate of calium carbonate.

Also the results showed that the magnesium hydroxide deposition increased with the increase in the flow velocity due to the improvement of the heat transfer coefficient. However, calcium carbonate deposition decreased with the increase in the velocity. This was explained by the effect of the water salinity since another run was carried out at constant salinity showed that the deposition of calcium carbonate increased with the increase in the velocity.

The fouling process cannot be avoided under any efforts and thus schedule cleaning, chemically by the use of anti-scale agent or mechanically by the use of sponge balls, is required. However, the results showed that operating the MSF plant between 90 ^{o}C and 100 ^{o}C is an effective strategy to avoid fast increase in the fouling. In addition, the MSF plants should be operated at certain velocity to assure constant flow of the heat transfer to the brine inside the tubes.

The simulation results of the proposed model provided close picture to the behaviour of the fouling in real plants and this can make remarkable contribution to the efforts to reduce the fouling and decrease the overestimated design fouling factor and hence, reduce the cost of extra surface area. Due to the difficulties of conducting experiments on real plants, most of the experimental studies were carried out using small experiments or pilot devices. However, the complexity and nonlinearity of the MSF process due to the continuous change in the temperature and salinity makes such experiments useless in predicting the actual behaviour of the fouling. The only an inexpensive available solution that can cope with the change of the temperature and salinity is by the means of simulation. The proposed model was proved to be

capable to run under any range of data and process variables and can accurately predict the precipitation of calcium carbonate and magnesium hydroxide in heat exchanger surfaces.

Nomenclature

A	Debye-Huckel constant
C_b	Concentration of ions in the fluid (kg/m^3)
C_i	Concentration of ions at the solid-liquid surface (kg/m^3)
C_s	Saturation concentration (kg/m^3)
D	Diffusion coefficient (m^2/s)
D_h	Hydraulic diameter (m)
d	Tube diameter (m)
d_P	Crystal size (m)
E_a	Reaction activation energy (kJ/mol)
f	Friction factor
g	Gravitational acceleration (m/s^2)
h	Heat transfer coefficient (kW/m^{2o}.K)
I	Ionic strength (mol/kg)
i	Inner
K	Proportional constant
k_D	Pre-exponent coefficient (m^4/s.kg)
k_r	Reaction rate constant (m^4/s.kg)
k_{rem}	Removal rate constant (m^3/s.kg)
K_{r0}	Pre-exponential constant (m^4/s.kg)
k_{sp}	Solubility product (mol^2/kg^2)
k_t	Conductivity of the tube material (kW/m^o.K)
K_w	Dissociation constant for water (mole/kg)
K_1	First dissociation constant (mole/kg)
K_2	Second dissociation constant (mole/kg)

m_d	Deposit mass rate (kg/s.m^2)
m_f	Net deposit mass rate (kg/s.m^2)
m_i	Molality of ion i
m_r	Removal mass rate (kg/s.m^2)
N	Number of defects in the fouling layer
n	Reaction order
o	Outer
P	Intercrystalline adhesion force (N)
R	Gas constant (kJ/mole.K)
Re	Reynolds number
R_f	Fouling resistance (m^2.^{o}.K/kW)
S	Salt concentration (g/l)
Sc	Schmidt number
Sh	Sherwood number
TC	Total carbon dioxide (mole/kg)
TA	Total alkaline (mole/kg)
T_s	Surface temperature (^{o}C)
ΔT	Temperature difference (^{o}C)
U_0	Overall heat transfer coefficient (kW/m^{2o}C)
V	Friction velocity (m/s)
v	Fluid velocity (m/s)
x_f	Layer thickness (m)
z_i	Charge of the ion i

Greek letters

ΔT	Temperature difference within foiling layer (^{o}C)
β	Mass transfer coefficient (m/s)
γ	Activity coefficients.
λf	Conductivity of the fouling layer (kW/m.K)
λ_{solid}	Conductivity of the compact solid (kW/m.K)

λ_{water}	Conductivity of pore medium (kW/m.K)
μ_w	Viscosity of the fluid (N.s/m^2)
ρ_f	Density of the fouling layer (kg/m^3)
ρ_{solid}	Density of the compact solid of fouling layer (kg/m^3)
ρ_w	Density of the fluid (kg/m^3)
σ_f	Shear strength of the fouling layer (N/m^2)
τ_f	Surface shear stress of the bulk flow (N/m^2)
ω	Porosity

References

[1]   K. Al-Anezi and N. Hilal, "Scale formation in desalination plants: effect of carbon dioxide solubility," *Desalination,* vol. 204, pp. 385-402, 2007.

[2]   I. M. Mujtaba, "Keynote Lecture," presented at the CAPE FORUM, Thessaloniki, Greece, 2008.

[3]   I. M. Mujtaba, "Modelling Multi Stage Flash Desalination Process " in *Dynamic Process Modeling*. vol. 7, ed, 2009, p. 628.

[4]   J. S. Gill, "A novel inhibitor for scale control in water desalination," *Desalination,* vol. 124, pp. 43-50, 1999.

[5]   M. A.-K. Al-Sofi, "Fouling phenomena in multi stage flash (MSF) distillers," *Desalination,* vol. 126, pp. 61-76, 1999.

[6]   M. Al-Ahmad and F. A. Aleem, "Scale formation and fouling problems and their predicted reflection on the performance of desalination plants in Saudi Arabia," *Desalination,* vol. 96, pp. 409-419, 1994.

[7]   S. H. Najibi, H. Müller-Steinhagen, and M. Jamialahmadi, "Calcium sulphate scale formation during subcooled flow boiling," *Chemical Engineering Science,* vol. 52, pp. 1265-1284, 1997.

[8]   A. E. Al-Rawajfeh, S. Ihm, H. Varshney, and A. N. Mabrouk, "Scale formation model for high top brine temperature multi-stage flash (MSF) desalination plants," *Desalination,* vol. 350, pp. 53-60, 2014.

[9]   D. Freyer and W. Voigt, "Crystallization and phase stability of CaSO4 and CaSO4–based salts," *Monatshefte für Chemie/Chemical Monthly,* vol. 134, pp. 693-719, 2003.

[10]   H. Glade and A. E. Al-Rawajfeh, "Modeling of CO2 release and the carbonate system in multiple-effect distillers," *Desalination,* vol. 222, pp. 605-625, 3/1/ 2008.

[11]   A. Helalizadeh, H. Müller-Steinhagen, and M. Jamialahmadi, "Mixed salt crystallisation fouling," *Chemical Engineering and Processing: Process Intensification,* vol. 39, pp. 29-43, 2000.

[12]   V. Höfling, W. Augustin, and M. Bohnet, "Crystallization fouling of the aqueous two-component system CaSO 4/CaCO 3," 2003.

[13]   D. Q. Kern and R. E. Seaton, "Surface fouling: how to calculate limits," *Chem. Eng. Prog,* vol. 55, pp. 71-73, 1959.

[14]   K. G. Cooper, L. G. Hanlon, G. M. Smart, and R. E. Talbot, "A model for the fouling of MSF plants based on data from operating units," *Desalination,* vol. 47, pp. 37-42, 1983.

[15]   D. Hasson, M. Avriel, W. Resnick, T. Rozenman, and S. Windreich, "Mechanism of calcium carbonate scale deposition on heat-transfer surfaces," *Industrial & Engineering Chemistry Fundamentals,* vol. 7, pp. 59-65, 1968.

[16]   E. Gazit and D. Hasson, "Scale deposition from an evaporating falling film," *Desalination,* vol. 17, pp. 339-351, 1975.

[17]   J. Taborek, T. Aoki, R. B. Ritter, J. W. Palen, and J. G. Knudsen, "Predictive methods for fouling behavior," *CHEMICAL ENGINEERING PROGRESS, VOL 68, NO 7, P 69-78, JULY 1972. 17 FIG, 9 REF.,* 1972.

[18]   D. Hasson, H. Sherman, and M. Biton, "Prediction of Calcium Carbonate Scaling Rates," in *Proceedings of 6th International Symposium Fresh Water from the Sea*, 1978, pp. 193-199.

[19]   R. Sheikholeslami, "Calcium sulfate fouling-precipitation or particulate: a proposed composite model," *Heat Transfer Engineering,* vol. 21, pp. 24-33, 2000.

[20]   H. M. Müller-Steinhagen and C. A. Branch, "Influence of thermal boundary conditions on calcium carbonate fouling in double pipe heat exchangers: Einfluβ der thermischen Randbedingungen auf die Ablagerung von CaCO3 in Doppelrohrwärmeübertragern," *Chemical Engineering and Processing: Process Intensification,* vol. 24, pp. 65-73, 1988.

[21]   A. Mubarak, "A kinetic model for scale formation in MSF desalination plants. Effect of antiscalants," *Desalination,* vol. 120, pp. 33-39, 1998.

[22]   F. Brahim, W. Augustin, and M. Bohnet, "Numerical simulation of the fouling process," *International Journal of Thermal Sciences,* vol. 42, pp. 323-334, 2003.

[23]   M. W. Bohnet, "Crystallization fouling on heat transfer surfaces–25 years research in Braunschweig," 2005.

[24]   M. G. Mwaba, M. R. Golriz, and J. Gu, "A semi-empirical correlation for crystallization fouling on heat exchange surfaces," *Applied Thermal Engineering,* vol. 26, pp. 440-447, 2006.

[25]   A. E. Al-Rawajfeh, "Simultaneous desorption–crystallization of CO2–CaCO3 in multi-stage flash (MSF) distillers," *Chemical Engineering and Processing: Process Intensification,* vol. 47, pp. 2262-2269, 2008.

[26]   R. Segev, D. Hasson, and R. Semiat, "Rigorous modeling of the kinetics of calcium carbonate deposit formation," *AIChE Journal,* vol. 58, pp. 1222-1229, 2012.

[27]   F. Zhang, J. Xiao, and X. D. Chen, "Towards predictive modeling of crystallization fouling: A pseudo-dynamic approach," *Food and Bioproducts Processing,* vol. 93, pp. 188-196, 2015.

[28]   A. M. Helal, "Uprating of Umm Al Nar East 4–6 MSF desalination plants," *Desalination,* vol. 159, pp. 43-60, 2003.

[29]   O. A. Hamed and H. A. Al-Otaibi, "Prospects of operation of MSF desalination plants at high TBT and low antiscalant dosing rate," *Desalination,* vol. 256, pp. 181-189, 2010.

[30]   E. A. M. Hawaidi and I. M. Mujtaba, "Simulation and optimization of MSF desalination process for fixed freshwater demand: Impact of brine heater fouling," *Chemical Engineering Journal,* vol. 165, pp. 545-553, 2010.

[31]   S. Said, I. M. Mujtaba, and M. Emtir, "Effect of Fouling Factors on the Optimisation of MSF Desalination Process for Fixed Water Demand Using gPROMS," in *Proceeding of the 9th International Conference on Computational Management*, London, UK, 2012.

[32] M. R. Malayeri and H. Müller-Steinhagen, "An overview of fouling mechanisms, prediction and mitigation strategies for thermal desalination plants," 2007.

[33] M. A. Soliman, "A MATHEMATICAL-MODEL FOR MULTISTAGE FLASH DESALINATION PLANTS," *JOURNAL OF ENGINEERING SCIENCES,* vol. 7, pp. 143-150, 1981.

[34] F. Fahiminia, A. P. Watkinson, and N. Epstein, "Early events in the precipitation fouling of calcium sulphate dihydrate under sensible heating conditions," *The Canadian Journal of Chemical Engineering,* vol. 85, pp. 679-691, 2007.

[35] N. Andritsos, "Calcium carbonate deposit formation under isothermal conditions," *Canadian journal of chemical engineering,* vol. 74, pp. 911-919, 1996.

[36] W. Augustin and M. Bohnet, "Influence of the ratio of free hydrogen ions on crystallization fouling," *Chemical Engineering and Processing: Process Intensification,* vol. 34, pp. 79-85, 1995.

[37] T. M. Pääkkönen, M. Riihimäki, C. J. Simonson, E. Muurinen, and R. L. Keiski, "Crystallization fouling of CaCO 3–analysis of experimental thermal resistance and its uncertainty," *International Journal of Heat and Mass Transfer,* vol. 55, pp. 6927-6937, 2012.

[38] B. R. Smith and F. Sweett, "The crystallization of calcium sulfate dihydrate," *Journal of Colloid and Interface Science,* vol. 37, pp. 612-618, 1971.

[39] M. Bohnet, "Fouling of heat transfer surfaces," *Chemical engineering & technology,* vol. 10, pp. 113-125, 1987.

[40] A. Helalizadeh, H. Müller-Steinhagen, and M. Jamialahmadi, "Mathematical modelling of mixed salt precipitation during convective heat transfer and sub-cooled flow boiling," *Chemical engineering science,* vol. 60, pp. 5078-5088, 2005.

[41] T. M. Pääkkönen, M. Riihimäki, C. J. Simonson, E. Muurinen, and R. L. Keiski, "Modeling CaCO 3 crystallization fouling on a heat exchanger surface–Definition of fouling layer properties and model parameters," *International Journal of Heat and Mass Transfer,* vol. 83, pp. 84-98, 2015.

[42] L. N. Plummer and E. Busenberg, "The solubilities of calcite, aragonite and vaterite in CO 2-H 2 O solutions between 0 and 90 C, and an evaluation of the aqueous model for the system CaCO 3-CO 2-H 2 O," *Geochimica et Cosmochimica Acta,* vol. 46, pp. 1011-1040, 1982.

[43] L. Sung-Tsuen and G. H. Nancollas, "The crystallization of magnesium hydroxide," *Desalination,* vol. 12, pp. 75-84, 2// 1973.

[44] S. K. Myasnikov, A. P. Chipryakova, and N. N. Kulov, "Kinetics, energy characteristics, and intensification of crystallization processes in chemical precipitation of hardness ions," *Theoretical Foundations of Chemical Engineering,* vol. 47, pp. 505-523, 2013.

[45] A. Eid Al-Rawajfeh, "Modeling of alkaline scale formation in falling film horizontal-tube multiple-effect distillers," *Desalination,* vol. 205, pp. 124-139, 2007.

[46] M. M. Awad, *Fouling of heat transfer surfaces*: INTECH Open Access Publisher, 2011.

[47] W. ElMoudir, M. ElBousiffi, and S. Al-Hengari, "Process modelling in desalination plant operations," *Desalination,* vol. 222, pp. 431-440, 2008.

[48] S. M. Alsadaie and I. M. Mujtaba, "Modelling and Simulation of MSF Desalination Plant: The Effect of Venting System Design for Non-Condensable Gases," *CHEMICAL ENGINEERING,* vol. 39, 2014.

[49] T. M. Pääkkönen, M. Riihimäki, E. Puhakka, E. Muurinen, C. J. Simonson, and R. L. Keiski, "Crystallization fouling of CaCO 3—effect of bulk precipitation on mass deposition on the heat transfer surface," 2009.

[50]   A. M. S. El Din and R. A. Mohammed, "Brine and scale chemistry in MSF distillers," *Desalination,* vol. 99, pp. 73-111, 1994.

[51]   R. Dooly and J. Glater, "Alkaline scale formation in boiling sea water brines," *Desalination,* vol. 11, pp. 1-16, 1972.

[52]   C. Wildebrand, H. Glade, S. Will, M. Essig, J. Rieger, K.-H. Büchner, *et al.*, "Effects of process parameters and anti-scalants on scale formation in horizontal tube falling film evaporators," *Desalination,* vol. 204, pp. 448-463, 2007.

[53]   A. Mucci, "The solubility of calcite and aragonite in seawater at various salinities and temperatures, and one atmosphere total pressure," *American Journal of Science,* vol. 283, pp. 780-799, 1983.

[54]   S. M. Peyghambarzadeh, A. Vatani, and M. Jamialahmadi, "Application of asymptotic model for the prediction of fouling rate of calcium sulfate under subcooled flow boiling," *Applied Thermal Engineering,* vol. 39, pp. 105-113, 2012.

[55]   A. M. Helal, A. Al-Jafri, and A. Al-Yafeai, "Enhancement of existing MSF plant productivity through design modification and change of operating conditions," *Desalination,* vol. 307, pp. 76-86, 2012.

[56]   S. A. Abdul-Wahab, K. V. Reddy, M. A. Al-Weshahi, S. Al-Hatmi, and Y. M. Tajeldin, "Development of a steady-state mathematical model for multistage flash (MSF) desalination plant," *International Journal of Energy Research,* vol. 36, pp. 710-723, 2012.

[57]   P. Fiorini and E. Sciubba, "Thermoeconomic analysis of a MSF desalination plant," *Desalination,* vol. 182, pp. 39-51, 2005.

[58]   V. M. Maniar and P. B. Deshpande, "Advanced controls for multi-stage flash (MSF) desalination plant optimization," *Journal of process control,* vol. 6, pp. 49-66, 1996.

[59]   O. A. Hamed, M. A. K. Al-Sofi, G. M. Mustafa, and A. G. Dalvi, "The performance of different anti-scalants in multi-stage flash distillers," *Desalination,* vol. 123, pp. 185-194, 1999.